Check for updates

Elongation of wood fibers combines features of diffuse and tip growth

Mateusz Majda[1,2] (iD), Liudmila Kozlova[1,3] (iD), Alicja Banasiak[1,4] (iD), Marta Derba-Maceluch[1] (iD), Igor A. Iashchishyn[5] (iD), Ludmilla A. Morozova-Roche[5] (iD), Richard S. Smith[2] (iD), Tatyana Gorshkova[3] (iD) and Ewa J. Mellerowicz[1] (iD)

[1]Department of Forest Genetics and Plant Physiology, Umeå Plant Science Centre (UPSC), Swedish University of Agricultural Sciences, Umeå 901 83, Sweden; [2]Department of Computational and Systems Biology, John Innes Centre, Norwich Research Park, Colney Lane, Norwich, NR4 7UH, UK; [3]Kazan Institute of Biochemistry and Biophysics, FRC Kazan Scientific Centre, Russian Academy of Sciences, Kazan 420111, Russia; [4]Department of Plant Developmental Biology, Institute of Experimental Biology, University of Wrocław, Kanonia 6/8, Wrocław 50-328, Poland; [5]Department of Medical Biochemistry and Biophysics, Umeå University, Umeå SE-901 87, Sweden

Authors for correspondence:
Mateusz Majda
Email: Mateusz.Majda@jic.ac.uk

Ewa J. Mellerowicz
Email: Ewa.Mellerowicz@slu.se

Summary

• Xylem fibers are highly elongated cells that are key constituents of wood, play major physiological roles in plants, comprise an important terrestrial carbon reservoir, and thus have enormous ecological and economic importance. As they develop, from fusiform initials, their bodies remain the same length while their tips elongate and intrude into intercellular spaces.
• To elucidate mechanisms of tip elongation, we studied the cell wall along the length of isolated, elongating aspen xylem fibers and used computer simulations to predict the forces driving the intercellular space formation required for their growth.
• We found pectin matrix epitopes (JIM5, LM7) concentrated at the tips where cellulose microfibrils have transverse orientation, and xyloglucan epitopes (CCRC-M89, CCRC-M58) in fiber bodies where microfibrils are disordered. These features are accompanied by changes in cell wall thickness, indicating that while the cell wall elongates strictly at the tips, it is deposited all over fibers. Computer modeling revealed that the intercellular space formation needed for intrusive growth may only require targeted release of cell adhesion, which allows turgor pressure in neighboring fiber cells to 'round' the cells creating spaces.
• These characteristics show that xylem fibers' elongation involves a distinct mechanism that combines features of both diffuse and tip growth.

Introduction

In stark contrast to animal cells, plant cells adhere to each other by the wall and growth must be synchronized with neighboring cells (Green, 1962; Guerriero *et al.*, 2014). This is called symplastic growth (Priestley, 1930), and it can be isotropic, with cells growing equally in all directions, or anisotropic, where cells grow more in certain directions. The latter is exemplified by cell growth during internode or hypocotyl elongation (Gendreau *et al.*, 1997), and growth of epidermal pavement cells leading to the formation of jigsaw puzzle-like cell shapes (Mathur, 2004).

Some cells, however, do not exhibit symplastic growth. For example some epidermal cells such as root hairs or trichomes grow protrusively, resulting in outgrowths that extend above the plant surface and are not limited by the surrounding cells (Guimil & Dunand, 2007; Kasili *et al.*, 2011; Yanagisawa *et al.*, 2015). Other cells grow intrusively, as their directional expansion leads to invasion of the middle lamella joining adjacent cells and breakage of plasmodesmatal contacts between them (Priestley, 1930; Sinnott & Bloch, 1939; Lev-Yadun, 2001). The intrusive growth through the tissue of transmitting tracts allows pollen tubes to reach micropyles of ovules and accomplish fertilization (Cheung, 1996; Smith & Oppenheimer, 2005). The process also occurs during differentiation of laticifers, sclereids (Lev-Yadun, 2001) and both phloem and xylem fibers (Sinnott & Bloch, 1939; Larson, 1994; Gorshkova *et al.*, 2012). Cell wall remodeling enzymes that participate in regulation of intrusive growth of xylem fibers have been identified (Gray-Mitsumune *et al.*, 2004, 2008; Siedlecka *et al.*, 2008; Kushwah *et al.*, 2020). Phloem fiber elongation has also been subjected to extensive microscopic (Esau, 1943; Ageeva *et al.*, 2005; Snegireva *et al.*, 2015) and transcriptomic analyses (Roach & Deyholos, 2008; Gorshkova *et al.*, 2018). However, the mechanism underlying this type of growth is still poorly understood.

It is generally assumed that xylem and phloem fibers elongate through apical intrusive growth whereby the middle part of fibers remains in contact with adjacent cells and does not elongate, while their tips form new cell wall material and intrude into the space between the adjacent cells (Sinnott & Bloch, 1939; Esau, 1953; Larson, 1994; Lev-Yadun, 2001). However, the

mechanisms of cell wall deposition and elongation at the tips are elusive. Phloem fibers of flax and hemp elongate at the primary wall stage by diffuse rather than tip growth (Gorshkova *et al.*, 2003; Ageeva *et al.*, 2005; Snegireva *et al.*, 2015). Three-dimensional reconstructions of elongating xylem fibers have shown that the tips frequently grow between tangential walls, starting at the three- or four-way junctions between the fibers which undergo radial expansion (Wenham & Cusick, 1975; Włoch *et al.*, 2009; Wilczek *et al.*, 2018). It is unknown what drives the cell separation where the tips intrude. It is also unclear if the fiber tip elongation uses a similar mechanism to moss protonema, root hairs and pollen tubes (Schiefelbein & Somerville, 1990; Parker *et al.*, 2000; Park *et al.*, 2011; Gu & Nielsen, 2013) or rather a diffuse growth mechanism as proposed for the phloem fibers (Gorshkova *et al.*, 2012).

To address these uncertainties, we used aspen as a model hardwood species to investigate the nature of secondary xylem fibers' intrusive growth. To determine if the elongation of the fibers occurs via tip or diffuse growth, we investigated cell wall architecture and composition along the length of developing fibers. Complementary approaches involving histochemistry, immunogold labeling, high-resolution atomic-force microscopy (AFM), and scanning electron microscopy (SEM) analyses revealed that clear differences exist in cell wall structure and composition between tips, the remaining part of extremities and bodies, suggesting most likely regions of cell wall extension. To determine how the intercellular spaces for tip intrusion could have been created among differentiating fibers, we used mathematical modeling, which allowed us to define conditions sufficient for intercellular space formation. The acquired data pave the way for research to understand the phenomenon of apical intrusive growth of xylem fibers.

Materials and Methods

Plant materials and isolation of wood samples

Hybrid aspen (*Populus tremula* L. × *tremuloides* Michx.) clone T89 trees were grown in the glasshouse as described previously (Derba-Maceluch *et al.*, 2015). Samples were collected from at least 10 trees (height > 1.5 m). Stem segments *c.* 14 mm long were dissected from the middle of internodes 41 and 42, which had *c.* 1 cm diameters. The segments were cut as shown in Fig. 1(a) fixed for 3 d in FAA (formaldehyde : glacial acetic acid : 50% ethyl alcohol, 0.5 : 0.5 : 9.0, v/v), and kept in 70% EtOH until use. The expanding developing secondary xylem (DX) was dissected after bark peeling (Gray-Mitsumune *et al.*, 2004). To prepare mature xylem samples (MX), wood *c.* 3–5 mm from the cambium was isolated.

Isolation of xylem fibers

Developing xylem and MX samples were incubated in maceration solution (30% H_2O_2 : glacial acetic acid, 2 : 1 v/v) at 90°C with periodic vigorous shaking until disintegration of the tissue (Siedlecka *et al.*, 2008), *c.* 2.5 h for DX and 5 h for MX. Fibers

were sedimented by low-speed centrifugation and stored in 70% ethanol at 4°C after a serial exchange of ethanol-water solutions.

A droplet of fiber suspension was dispersed in 1 ml water in a 2 ml Eppendorf tube and used for immunolocalization studies. Another droplet was placed on a poly-L-lysine-coated glass slide and dried on the warming plate for microscopy analyses.

Resin embedding

Pieces of internode segments (*c.* 1 × 1 × 1 mm) were fixed in ice-cold fixative (4% paraformaldehyde, 0.05% glutaraldehyde, 100 mM phosphate buffer, pH 7.2) at 4°C overnight, washed with 100 mM phosphate buffer followed by distilled water, dehydrated in an ethanol series and embedded in medium hardness LRW resin (TAAB Laboratories Equipment Ltd, Aldermaston, UK). Ultrathin cross-sections (70 nm thick) for transmission electron microscopy (TEM) and 1-µm-thick sections for light microscopy (LM) were prepared using an ultramicrotome (RMC Power Tome; Boeckeler Instruments, Tucson, AZ, USA) and/or Reichert Ultracut Microtome (Reichert-Jung Inc., Buffalo, NY, USA). Sections for TEM were mounted on formvar-coated grids (Majda, 2019), and sections for light microscopy were placed on poly-L-lysine-coated glass slides then dried on a warming plate.

Anatomical studies

Resin-embedded cross-sections and macerated wood fibers were stained with toluidine blue or with a combination of safranin and alcian blue. Images were then acquired using a Zeiss Axiovert microscope (Carl Zeiss, Jena, Germany) equipped with a charge-coupled device (CCD) camera.

Immunolocalization studies with isolated fibers

Macerated cell suspensions in Eppendorf tubes were subjected to brief sedimentation with a bench centrifuge, the water was replaced with 100 mM phosphate-buffered saline (PBS), pH 7.2, followed by 50 mM glycine in PBS, and (15 min later) a blocking reagent (3% bovine serum albumin (BSA) in PBS). After 30 min, samples were incubated for 60 min in primary antibodies (Table 1) in PBS containing 1% BSA and 0.05% Tween-20. The macerates were washed three times in 1% BSA solution alone, then incubated for 60 min in 1% BSA solution with corresponding secondary antibodies. After two washes with 1% BSA, two with PBS, and water, the samples were incubated for 10 min in a silver enhancer kit (BBInternational, Cardiff, UK) for visualization in light microscopy and washed again in distilled water. A droplet of the suspension was then placed on a slide and observed under a Zeiss Axiovert microscope with a CCD camera. The measurements were performed using FIJI (https://fiji.sc). Each fiber was classified according to its labeling type (Supporting Information Fig. S4).

Immunogold labeling for transmission electron microscopy

Grids with the stem sections were incubated in a 1% BSA in 100 mM PBS for 15 min, followed by this solution
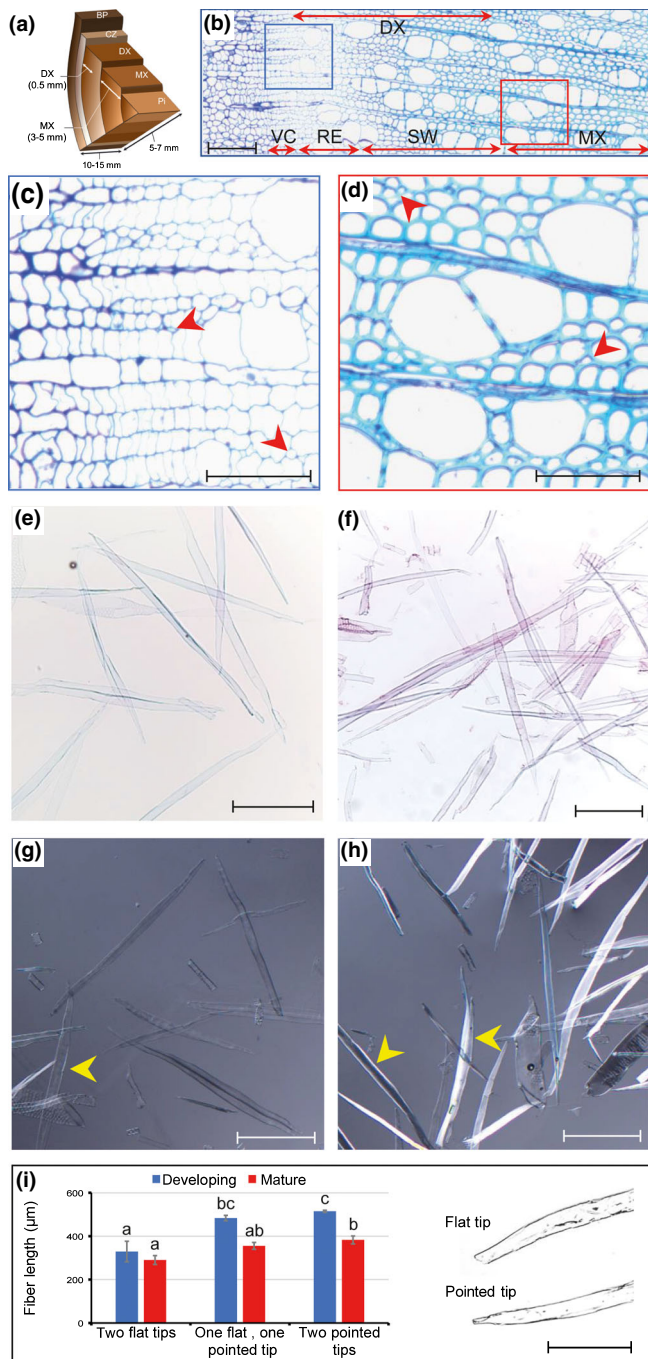
Fig. 1 Anatomy of developing and mature xylem fibers of hybrid aspen. (a) Sampling scheme. BP, bark and phloem; CZ, cambial zone; DX, developing xylem; MX, mature xylem; Pi, pith. (b) Anatomy of DX and MX xylem. VC, vascular cambium; RE, radial expansion zone; SW, secondary wall deposition zone. (c, d) Higher magnification micrographs of parts shown in insets in (b). Red arrows point to fiber tips. (e, f) Safranin-alcian blue staining of fibers isolated from DX (e) and MX (f). (g, h) Nomarski images of unstained fibers from DX (g) and MX (h). Yellow arrows show the brighter signals from cell walls of fiber bodies than from their tips. (i) Lengths of fibers with indicated tip morphologies. Data are means ± SE. Significant differences between the means are indicated by different letters (according to one-way ANOVA followed by Tukey test, $P < 0.01$, $n = 50$ for developing fibers and 67 for mature fibers). Bars: (c, d) 50 μm; (b, i) 100 μm; (e–h) 200 μm.

supplemented with JIM5 primary antibody (Table 1) for 45 min, washed in PBS and incubated with the corresponding secondary antibody (Table 1) in 1% BSA in PBS for 60 min. The samples were subsequently rinsed with 1% BSA in PBS, PBS and distilled water, then left to dry on filter paper. For visualization by TEM, the sections were incubated with 5% uranyl acetate for 10 min, rinsed in tap water and left to dry on a filter paper. Images were acquired using a Jeol 1230 TEM (Jeol, Ltd, Tokyo, Japan; accelerating voltage 80 kV with a Gatan MSC 600CW (Gatan, Warrendale, PA, USA) 2k × 2k CCD camera).

Scanning electron microscopy

A droplet of macerated material in water (immunolabeled without using the silver-enhancing kit) was placed on MAS-GP™ hydrophilic adhesion microscope slides (Matsunami Glass Ind. Ltd, Osaka, Japan) and left until dry. The material that adhered to the slides was treated with a 1% uranyl acetate aqueous solution (10 min) and a 1% lead citrate aqueous solution (5 min). Samples (10 mm²) were obtained from the slides using a diamond pen and positioned on an aluminum stub by carbon tape. Coating of the material (1 nm thick layer of carbon) was performed with a dual carbon/sputter coater (Quorum Q150T-ES & Edwards S150A; Quorum Technologies, Lewes, UK).

Material that adhered to the slides was stained with a 1% aqueous solution of uranyl acetate (for 10 min) and a 1% aqueous solution of lead citrate (for 5 min). The glass slides with the material were cut into 10 mm² pieces using a diamond pen and mounted on an aluminum stub with carbon tape. The material was then coated with a 1-nm-thick layer of carbon using a dual carbon/sputter coater (Quorum Q150T-ES & Edwards S150A). Images of the fibers were acquired using a Merlin field emission scanning electron microscope (Merlin FE-SEM; Carl Zeiss). Images of regions of interest were acquired using an energy-selective backscattered (EsB) detector, with accelerating voltages of 7 and 3 kV.

For observation of cellulose microfibrils, macerated fibers of three trees were suspended in 70% ethanol and gradually dehydrated up to 96% ethanol. Each suspension was cast on an aluminum stub, critical point-dried using a Leica EM CPD300 instrument, and coated with 5 nm iridium using a Quorum Q150T-ES sputter coater. For imaging, the Zeiss Merlin FE-SEM was used with 2 kV accelerating voltage. Microfibril angles were measured using on-screen PROTRACTOR v.5.0 software.

Atomic force microscopy

A drop containing suspension of macerated fibers was placed on a glass slide and air-dried. Individual fibers were measured at room temperature in the air, using a NTEGRA Prima (NT-MDT, Zelenograd, Russia) scanning probe microscope in semi-contact mode to characterize their topography. The probes used (HA-HR, NT-MDT) have a c. 380 kHz resonance frequency, a

Table 1 Primary and secondary antibodies used in the study.

Antibodies	Specificity	Source
Mouse monoclonal CCRC-M1	Fucosylated XG	CarboSource
Mouse monoclonal CCRC-M58	Nonfucosylated XG	CarboSource
Mouse monoclonal CCRC-M89	Nonfucosylated XG	Carbosource
Rat monoclonal JIM5	Low methyl-esterified HG	PlantProbes
Rat monoclonal JIM7	High methyl-esterified HG	PlantProbes
Rat monoclonal LM5	(1-4)-β-galactan	PlantProbes
Rat monoclonal LM6	(1-5)-α-arabinan	PlantProbes
Rat monoclonal LM7	Low methyl-esterified HG	PlantProbes
Rat monoclonal LM10	Xylan	PlantProbes
Rat monoclonal LM11	Xylan and arabinoxylan	PlantProbes
Rat monoclonal LM21	Heteromannan	PlantProbes
Rat monoclonal LM23	Nonacetylated xylosyl	PlantProbes
EM Goat anti-Mouse IgG: 10 nm Gold	Mouse IgG, monoclonal	BBInternational
EM Goat anti-Rat IgG: 10 nm Gold	Rat IgG, monoclonal	BBInternational

HG, homogalacturonan; IgG, immunoglobulin G; XG, xyloglucan.

$c.$ 34 N m^{-1} spring constant and a 10 nm apex radius. The average scanning area was 50 μm^2, and the scanning rate was 0.3 Hz. Measurements of minimal height and width were acquired from height profiles taken perpendicularly to the longitudinal axis of each examined fiber, at 10 μm intervals along its entire length, avoiding pits.

Results

Developing and mature xylem fibers have distinct anatomical features

Meristematic activity of the vascular cambium results in inward production of secondary xylem and outward production of secondary phloem (Fig. 1a,b). To follow the development of xylem fibers, we isolated cells from the DX and the MX close to the pith (Fig. 1a–d). Light microscopy images of macerated fibers indicated a clear difference in fiber appearance between the DX (Fig. 1e,g) and MX zones (Fig. 1f,h). Developing xylem samples included fibers with thin cell walls, which were not lignified according to histological staining with safranin-alcian blue, and showed little contrast when viewed with Nomarski optics, while all fibers in MX samples had thick, lignified cell walls that were bright in Nomarski images (Fig. 1e–h). We concluded that developing fibers with only primary walls can be distinguished from fibers with secondary walls of the DX region using their anatomical features. Interestingly, the cell wall of the main bodies of some developing and mature fibers appeared thicker and more strongly lignified compared with tips, according to staining intensity (Fig. 1e,f) and contrast in Nomarski images (arrows in Fig. 1g, h). Thus, there appeared to be clear differences in cell wall properties between these fibers' tips and main bodies.

The fiber tip shape is an indicator of intrusive growth

Among the developing and mature fibers, we distinguished three populations: fibers with pointed, flat or mixed (one pointed and one flat) tips. Most fibers had either two (55%) or one (35%) pointed tips. Fibers with two flat tips were rarer (10%) and shorter than other fibers (Fig. 1i), suggesting that these fibers grew less than the others. The length of mature fibers was reduced compared with that of developing fibers. This is expected because the mature fibers differentiated from much shorter fusiform initials than the developing fibers, owing to large increases in fusiform initial length typical for aging of the young cambium (Larson, 1994).

Next, we examined differences in cell wall thickness between the fiber tips and bodies by anatomical observations. We analyzed the cell thickness of dried macerated fibers that had very little cell lumen (Fig. S1) by high-resolution AFM. The AFM height profiles across the fibers and perpendicular to their longitudinal axes included high zones at both edges corresponding to folded cell wall, and depressions indicating pits (Fig. S2). Therefore, the double cell wall thickness of an examined fiber could be approximated as the minimum height observed in an acquired profile with no depressions. We observed that the cell walls in mature fibers were approximately two times thicker than in developing fibers, confirming that the method could adequately detect developmental differences in cell wall thickness. In both developing and mature fibers, the cell walls were significantly thicker in the region of the main body than at the tips (Fig. 2a–c). In developing fibers, we found significant differences in cell wall thickness among the fiber main body, pointed tip and flat tip zones (mean values: $c.$ 145, 60 and 90 nm, respectively) (Fig. 2b). The difference between tips and the main bodies was maintained in mature fibers, indicating that following fiber expansion, the rate of cell wall biosynthesis is higher in the main fiber body than at the tips.

We also used AFM to measure the width of fibers along their lengths, and distances from the last pit to the tip. This revealed that thin-walled regions of the fibers correspond to regions where the fibers are narrow (Fig. 2c). These regions account for 20–30% of the total length of fibers with pointed tips, but just 5–10% of the length of fibers with flat tips. Further observations indicated that these regions correspond to the regions devoid of pits (Fig. S3), which is one of the characteristics of the intrusively grown part of the fiber (Larson, 1994; Chaffey et al., 1999). Thus, we called the zones with no pits, thin cell walls and narrow width 'fiber extensions' that elongated beyond their bodies by apical intrusive growth.

Spatial distributions of cell wall matrix components in young and mature fibers

To assess chemical differences between tips and bodies, we used 12 antibodies (Table 1) recognizing the most common cell wall epitopes of polysaccharide matrix components in aspen fibers (Mellerowicz & Gorshkova, 2012; Guedes et al., 2017) for immunogold labeling in isolated developing and

mature fibers. Although the isolation procedure would probably affect the labeling, we reasoned that all parts of fibers were subjected to the same treatment, so any differences in labeling along their lengths would support our hypothesis that the cell wall of elongating fibers is not homogeneous. We found four types of labeling: uniformly weak or uniformly strong labeling of the entire wall of the fibers, localized labeling associated with one or both of their tips (the most apical part of extensions) or labeling solely along fiber main bodies with none at the tips (Fig. S4a). Negative controls for epitopes recognized by the secondary antibodies alone revealed no labeling (Fig. S4b). The frequencies of these labeling patterns obtained with each antibody were used to classify the associated epitopes as having uniform distribution or differential distributions between tips and bodies of developing fibers.

Cell wall epitopes uniformly distributed in fibers from developing and mature wood

Uniformly weak labeling was observed in cell walls of both developing and mature xylem following treatments with half of the applied antibodies. These included xylan nonreducing end epitope (LM10) (Ruprecht *et al.*, 2017) (Fig. S5a,b,g,h,m), epitopes of xylan and arabinoxylan (LM11) (McCartney *et al.*, 2005) (Fig. S5c,d,i,j,n), and nonacetylated xylosyl residues in xylogalacturonan and xylan (LM23) (Pedersen *et al.*, 2012) (Fig. S5e,f,k,l,o). The weak labeling by these antibodies could have been a result of the association of their epitopes with secondary walls (McCartney *et al.*, 2005; Scheller & Ulvskov, 2010; Mellerowicz & Gorshkova, 2012; Guedes *et al.*, 2017), which are not exposed to antibodies in whole mount material such as macerated fibers.

Uniform weak labeling of both developing and mature fibers was also observed for pectic rhamnogalacturonan I (RGI)-related epitopes such as (1,4)-β-D-galactan nonreducing end (LM5) (Andersen *et al.*, 2016) (Fig. S6a,b,g,h,m) and (1,5)-α-L-arabinan epitopes (LM6) (Willats *et al.*, 1998; Lee *et al.*, 2005; Verhertbruggen *et al.*, 2009) (Fig. S6c,d,i,j,n), as well as heteromannan epitopes (LM21) (Marcus *et al.*, 2010) (Fig. S6e,f,k,l,o).

Tips of developing fibers are rich in homogalacturonan epitopes

Pectic homogalacturonan (HG) epitopes such as low methyl-esterified HG labeled by JIM5 (Fig. 3a,b,g,h,m) or LM7 (Fig. 3c, d,i,j,n) and high methyl-esterified HG (Fig. 3e,f,k,l,o) (Knox *et al.*, 1990; Willats *et al.*, 2000; Clausen *et al.*, 2003) displayed different distribution patterns from those observed for xylan, mannan and RGI. All investigated HG epitopes tended to be localized at tips of developing fibers (Fig. 3a,g,c,i,e,k), but uniformly distributed in mature fibers (Fig. 3b,h,d,j,f,l). The most pronounced tip-labeling pattern was recognized by JIM5, which was strongly localized at the tips in developing fibers (Fig. 3a,g) during the primary walled stage of their development (Fig. 4a; compare tips shown by blue and red arrows). However, JIM5 was sparsely but uniformly distributed in mature wood fibers (Fig. 3b,h). Scoring of the different labeling patterns showed that low methyl-esterified HG epitopes accumulated at one or both tips in > 60% of developing fibers (Fig. 3m). Low methyl-esterified HG epitopes labeled by LM7 and highly methyl-esterified epitopes were less abundant, but also accumulated at the tips of *c.* 60% and 20% of analyzed developing fibers, respectively, whereas in mature fibers these epitopes were uniformly distributed (Fig. 3n,o). The cell wall region that was highly labeled by JIM5 in pointed tip fibers extended to 17.5 ± 0.8 μm (mean $\pm$ SE, $n = 152$) from the apex rather than covering entire fiber extensions (Fig. 4a,b).

To verify that JIM5 antibodies bind cell wall epitopes at the cell surface and not inside the macerated fibers, we applied immunolocalization using high-resolution SEM. This analysis revealed the presence of JIM5 antibodies at the surface of developing fibers, and their low abundance at the surface of mature fibers (Fig. S7a,b).

To determine if the JIM5 epitopes have similar distributions in developing wood tissue that was not treated with maceration fluid, we studied ultrathin cross-sections of immunogold-labeled developing wood using high-resolution TEM (Fig. 4b,c). Developing fiber tips appear in such sections as densely cytoplasmic cells with small diameters (indicated by arrows in Fig. 4b) protruding between cells with wider lumens (Mellerowicz, 2006). JIM5 labeling was high in cell walls of these tips (Figs 4b,c, S8), but weaker in walls of the fiber bodies. Moreover, the distribution of label across the cell wall differed between fiber tips and bodies. The tips exhibited the most prominent labeling in the cell wall layer that was being deposited (adjacent to the plasma membrane), but the bodies had most label in the middle lamella. This underscores a unique character of the tip cell wall and suggests a prominent role for HG in fiber apical elongation.

Nonfucosylated xyloglucan epitopes are sparse at extensions of intrusively growing fibers

Immunolocalization of nonfucosylated xyloglucans (XGs; CCRC-M89 and M58 antibodies) (Pattathil *et al.*, 2010) revealed a distribution gradient along the length of developing fibers, and uniformly weak labeling in mature fibers (Fig. 5a–d, g–j,m,n). Main bodies of *c.* 60% of developing fibers were more strongly labeled than the tips with CCRC-M89 antibodies (Fig. 5m) and *c.* 30% with CCRC-M58 antibodies (Fig. 5n). CCRC-M58 labeling was much less intense (Fig. 5c,i). The CCRC-M89 label-free region in developing fibers with pointed tips extended to 48.3 ± 2.0 μm ($n = 104$) from the apex, covering a large part of fiber extensions (Fig. 5g).

Signals of fucosylated XGs (CCRC-M1) were sparse and uniformly distributed along the length of fibers in both developing and mature wood (Fig. 5e,f,k,l,o).

To confirm the surface localization of the CCRC-M89 antibody in the main body of developing fibers, we subjected isolated fibers to immunogold labeling and detected the label with high-resolution SEM. This analysis confirmed that the labeling was present at the cell surface in developing fibers, while it was barely detectable in mature fibers (Fig. S7c,d).
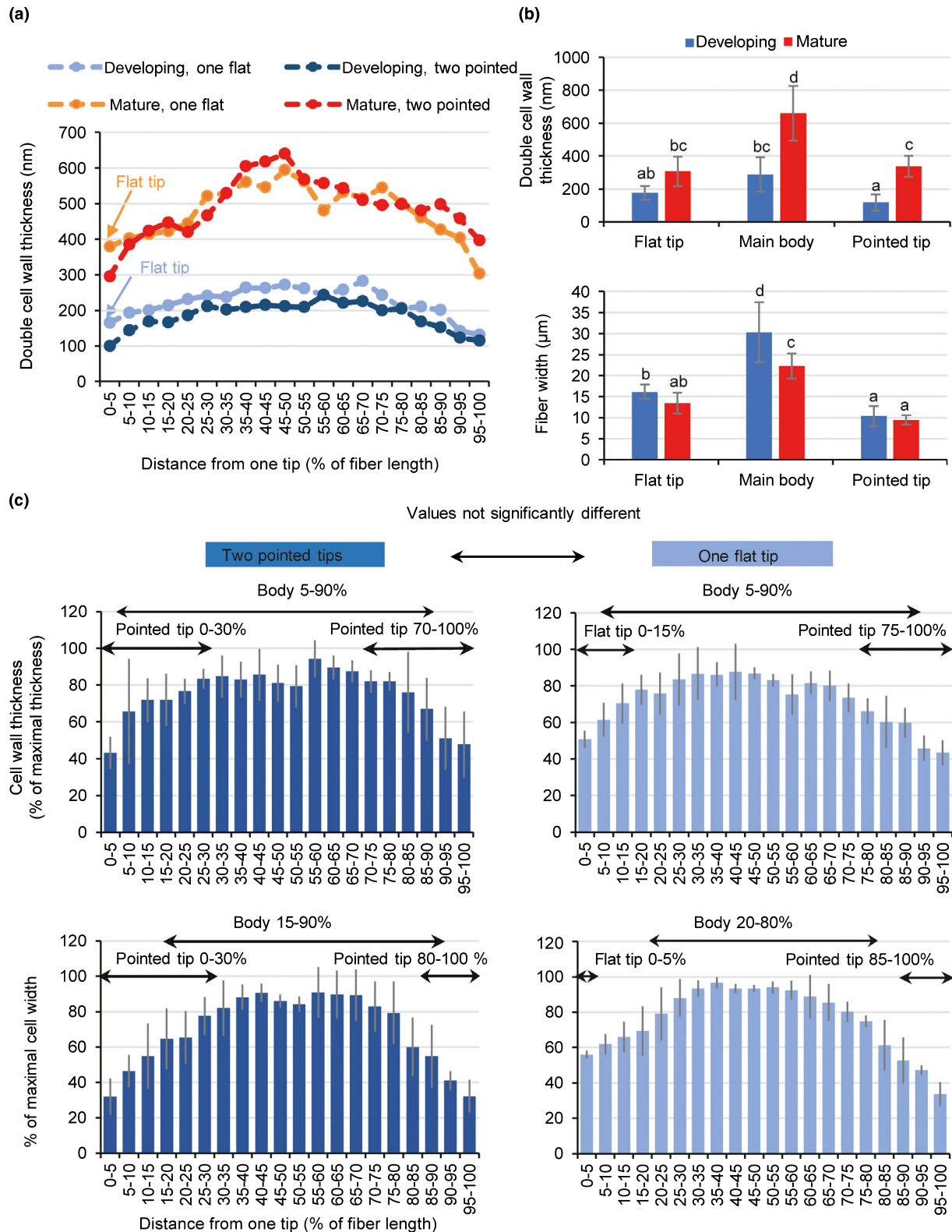
Fig. 2 Changes in cell wall thickness and width along the length of fibers determined by atomic-force microscopy (AFM) in identified types of fibers. (a) Examples of the double cell wall thickness profiles (estimated from height profiles by AFM) along the length of indicated types of developing and mature fibers. (b) Mean double cell wall thicknesses and widths at fibers' tips and bodies. The values for the fiber bodies were measured at the highest point along the fiber length. (c) Average profiles of cell wall thicknesses and widths along the lengths of developing fibers with one or two pointed tips. Data in (b) and (c) are means ± SD ($n = 9$). The significance of differences among the means is indicated by different letters and was tested by one-way ANOVA followed by the Tukey test at $P < 0.05$. Data for cells with two flat tips are not presented because they were rare.

Correlation of fiber labeling patterns with cell elongation

To clarify relationships between the nonuniform distributions of HG and nonfucosylated XG along the length of fibers and their intrusive growth, we measured lengths of developing fibers with polarized and uniform labeling patterns and scored their tip morphology as either pointed or flat. If a particular labeling pattern in fibers is associated with intrusive growth and disappears after elongation is finished, fibers displaying the pattern should be shorter than the others. Conversely, if a labeling pattern appears only after some elongation, or persists in fully elongated fibers, then the fibers showing it should be longer than the others. Fibers with pronounced JIM5 labeling at the tips were slightly longer than those with a uniform labeling pattern (Fig. 6a). Moreover, the uniformly labeled tips were usually (but not always) flat, whereas tips labeled with JIM5 predominantly had a pointed morphology (Fig. 6b). These data indicate the presence of JIM5 epitopes at the tips in both partially and fully elongated fibers. Fibers with uniform CCRC-M89 labeling were much shorter than those with a localized (body only) labeling pattern (Fig. 6a) and had slightly increased frequency of flat tip morphology (Fig. 6b). These results indicate that CCRC-M89 epitopes are excluded from the fiber extensions of elongated fibers.

Reorganization of cellulose microfibrils at the tips of elongating fibers

As we observed clear differences in distributions of matrix epitopes between fiber bodies and elongating tips, we wanted to see if the pattern of cellulose microfibril deposition was polarized. For this we used high-resolution SEM imaging to visualize the cellulose microfibril patterns in isolated fibers. In most developing and mature fibers with pointed tips, the orientation of cellulose close to the apex was highly ordered and transverse or helical with a large microfibril angle (MFA) and S-type chirality as defined by Wardrop & Harada (1965) (Fig. 7b,c,e,f,h, j,l,m). The flat tips did not have such transverse cellulose organization (Fig. 7k,m). Close to the tip, the transverse cellulose microfibrils were usually clearly visible, but the pattern became less clear within $15.2 \pm 1.0 \, \mu m$ ($n = 17$) from the tips of developing fibers, and $8.5 \pm 1.2 \, \mu m$ ($n = 11$) from the tips of mature fibers (blue and red arrows in Fig. 7l). Sometimes a distinct border was discernible between the tip-associated cell wall layer with transverse, clearly distinguishable microfibrils and the cell wall layer with disordered or cross-linked patterns (black arrows in Fig. 7b,d,e). The nearly transverse helix of cellulose microfibrils became steeper within a few μm of the tip in developing pointed fibers, and this change was more pronounced in mature fibers (Fig. 7l). The cellulose fibrils in fiber bodies lacked uniform orientation and looked cross-linked in developing fibers, while they were more clearly discernible as longitudinally arranged, but without a strongly coordinated pattern in mature fibers (Fig. 7g,i). As cellulose microfibrils constitute the major load-bearing component of the cell wall and determine its anisotropy, their organization into distinct domains with characteristic deposition patterns suggests anisotropic and tip-oriented growth of the fibers.

Mechanical modeling reveals that turgor pressure can generate intercellular spaces

As the fusiform cells are tightly connected to each other, we wanted to elucidate how the fibers' tips could grow between them, and particularly how the intercellular spaces are formed. Wenham & Cusick (1975) suggested that it was not possible for intrusive tips to be 'pushed' between cells, mechanically causing separation and displacement of their neighbors. They argue that differential turgor pressure is not a possible mechanism because cells can create a growing tip intruding their neighbors at one end while simultaneously being intruded at the other end. Instead they hypothesize that the spaces must be formed for the intruding tips to grow into by the separation of the middle lamella and their subsequent displacement by growth. Wenham & Cusick (1975) also comment that the tips have concave areas, an unusual shape for pressurized cells that also suggests the space defines their shape. To investigate this possibility, we constructed a computer model of the DX layer with cells subjected to turgor pressure. As the cells are greatly elongated, their mechanics can be reasonably well captured in a two-dimensional cross-section, which was modeled as a mass-spring system (see Methods S1; Mosca *et al.*, 2017, 2018) using the MORPHODYNAMX software (www.MorphoDynamX.org). The model consists of vertices (cell junctions and intermediate points) connected by springs (cell walls) with *c.* 500 nm spacing. The initial state of the model is slightly trapezoidal to represent the curvature of the cambium (Fig. 8a). The boundary on both sides is fixed to radial lines that allow vertices to move radially outwards away from the MX but not tangentially towards the sides, simulating the presence of a full ring of tissue. Vertices at the bottom of the structure are fixed in their radial coordinate to simulate connections to the inner woody tissue where the MX is located. Starting from almost square cells adhering to each other, as seen in cambium meristem and early expanding fibers (Fig. 8a), turgor pressure is applied to inflate the cells, resulting in radial expansion of the structure (Fig. 8b). Note the ballooning of the upper boundary layer cells in the simulation, as the free walls round up as a result of turgor pressure. In reality, this layer of cells would be some distance away; however, adding more layers does not affect space formation. After the cells are pressurized, the detachment of the middle lamella is simulated by separating the vertices close to the junctions of the cells. This causes the formation of intercellular spaces (Fig. 8c). Intuitively one might expect the cells to bulge into their neighbors if they are free to do so at the junctions, but the tension in the cell walls as a result of turgor pressure causes the cells to become rounder, and the whole structure expands radially and spaces appear. Although Wenham & Cusick (1975) hypothesize that radial growth is required after separation to open up the spaces, the model shows that this can happen as a purely elastic effect of separation of the pressurized cells. These possibilities are not in conflict as, in experimental measurement, elastic expansion would look the same as growth.
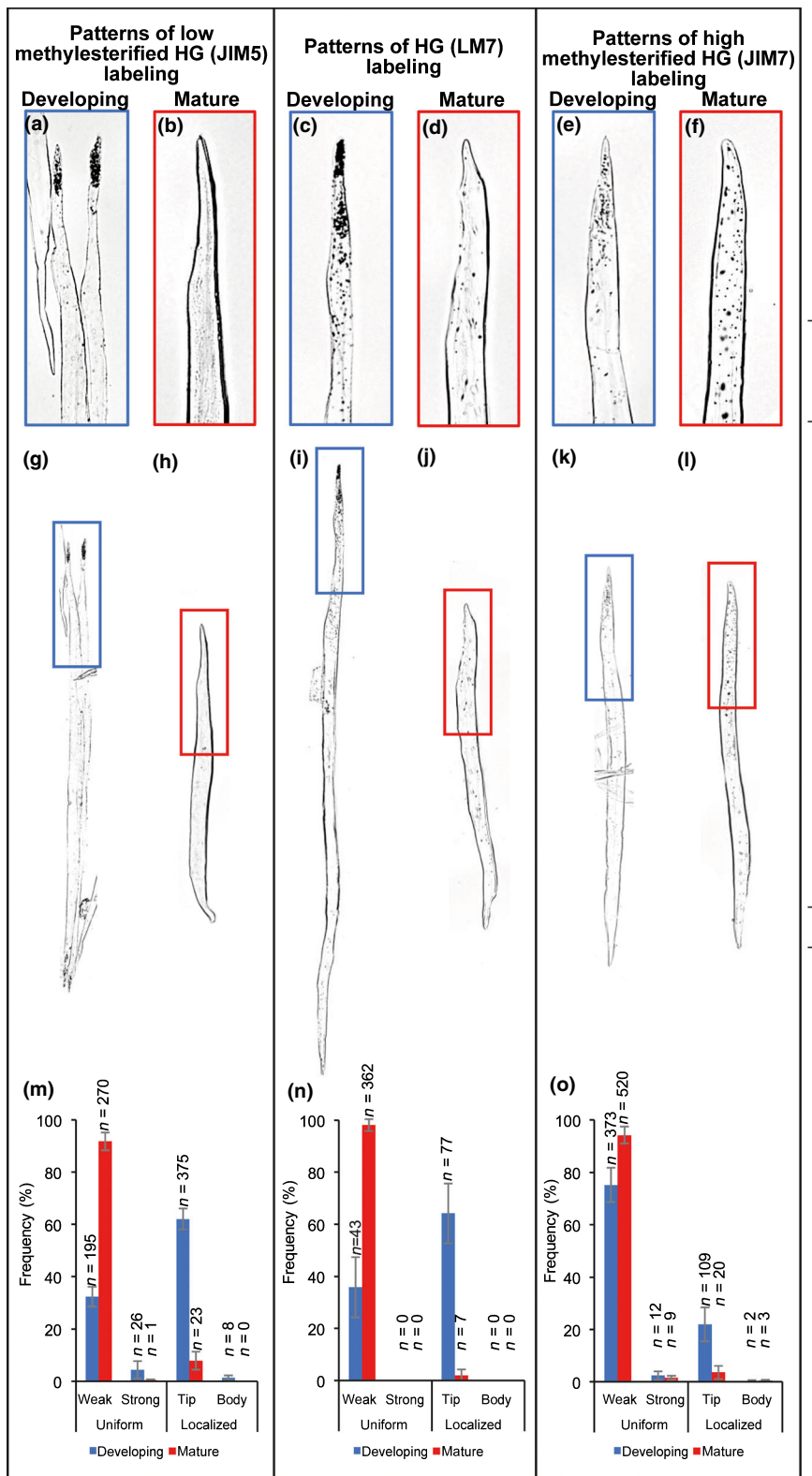
Fig. 3 Homogalacturonan (HG) epitopes accumulate at tips of developing fibers. (a–l) Representative images of developing and mature fibers immunolabeled (as manifested by black signal) with monoclonal antibodies recognizing indicated epitopes of HG. The upper panel presents high-resolution images of tips of the fibers shown in the lower panel. Bars, 50 μm. (m–o) Graphs showing percentages of fibers displaying indicated labeling patterns. Total numbers of analyzed fibers (*n*) are displayed on the bars. Data are means ± SE, calculated for independent immunolabeling experiments with developing and mature fibers (18 and nine experiments with JM5 antibodies, five and three with LM7 antibodies, 11 and seven with JM7 antibodies, respectively).

The model also has implications for the interpretation of growth directions in these cells, in particular of the nonintrusive growth of the fusiform initials. In the model it can been seen that when spaces open up, all the cells move outwards and, as with growth, the tissue expands mostly in the radial direction. This happens because the cells are constrained in the tangential direction. Nevertheless, expansion in the radial direction causes spaces to open up both in the radial and tangential directions. It has been suggested that intrusive growth cannot occur between radial walls (Jura *et al.* 2006;
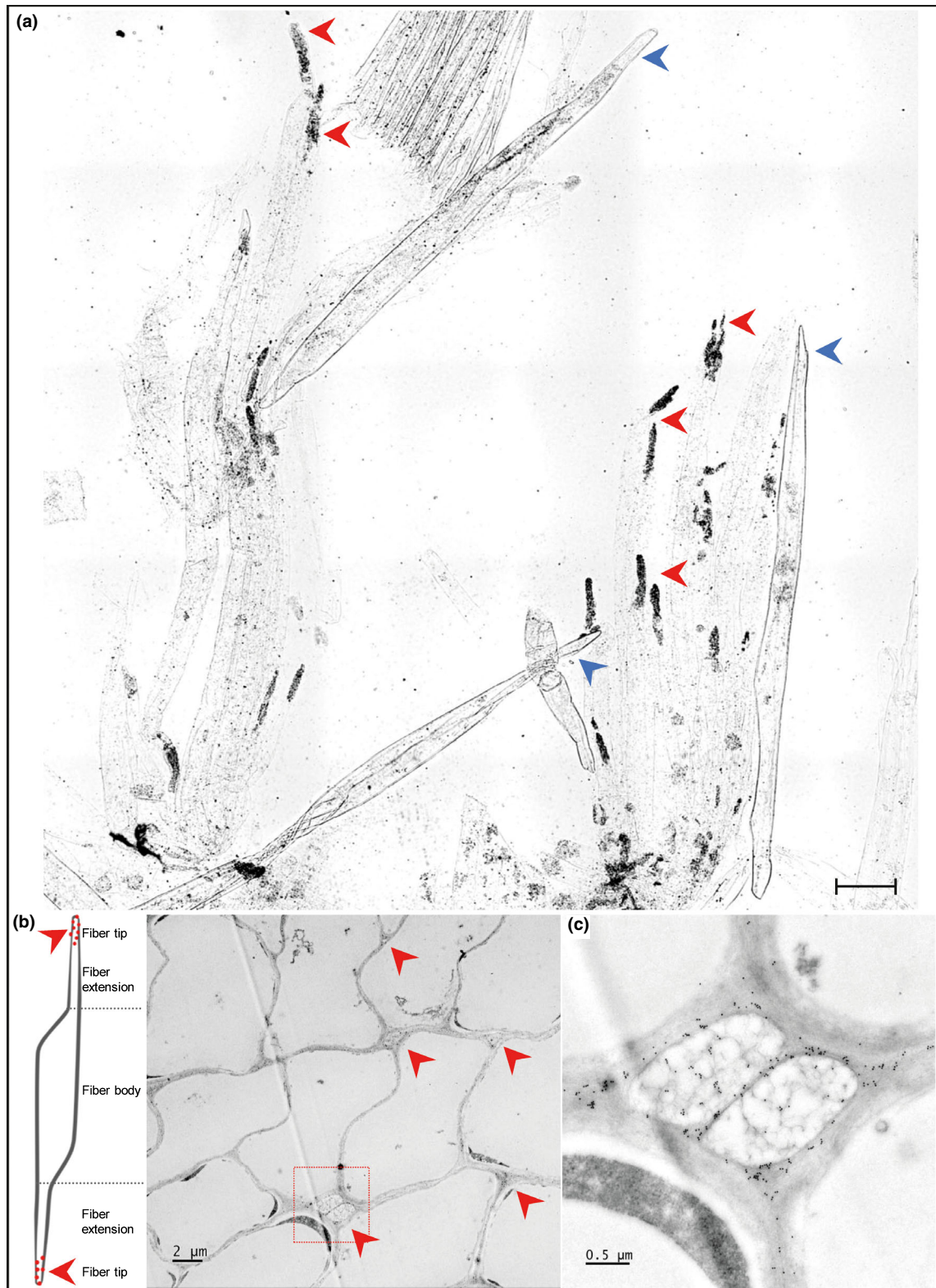
Fig. 4 Distribution of low methylesterified homogalacturonan epitopes across the cell wall of developing fibers. (a) Light microscopy image of JIM5 labeling in developing wood fibers. Note the apical accumulation of the antibody (black label) in the thin-walled fibers. Red arrows indicate fiber tips accumulating the label. Blue arrows show fiber tips devoid of the label, which were usually associated with thick-walled fibers. Bar, 50 μm. (b) Transmission electron micrographs showing JIM5 labeling in ultrathin section through the developing zone of the xylem. Red arrows indicate accumulation of the antibody at the tips of the fibers. (c) Zoomed image (red frame in (b)).
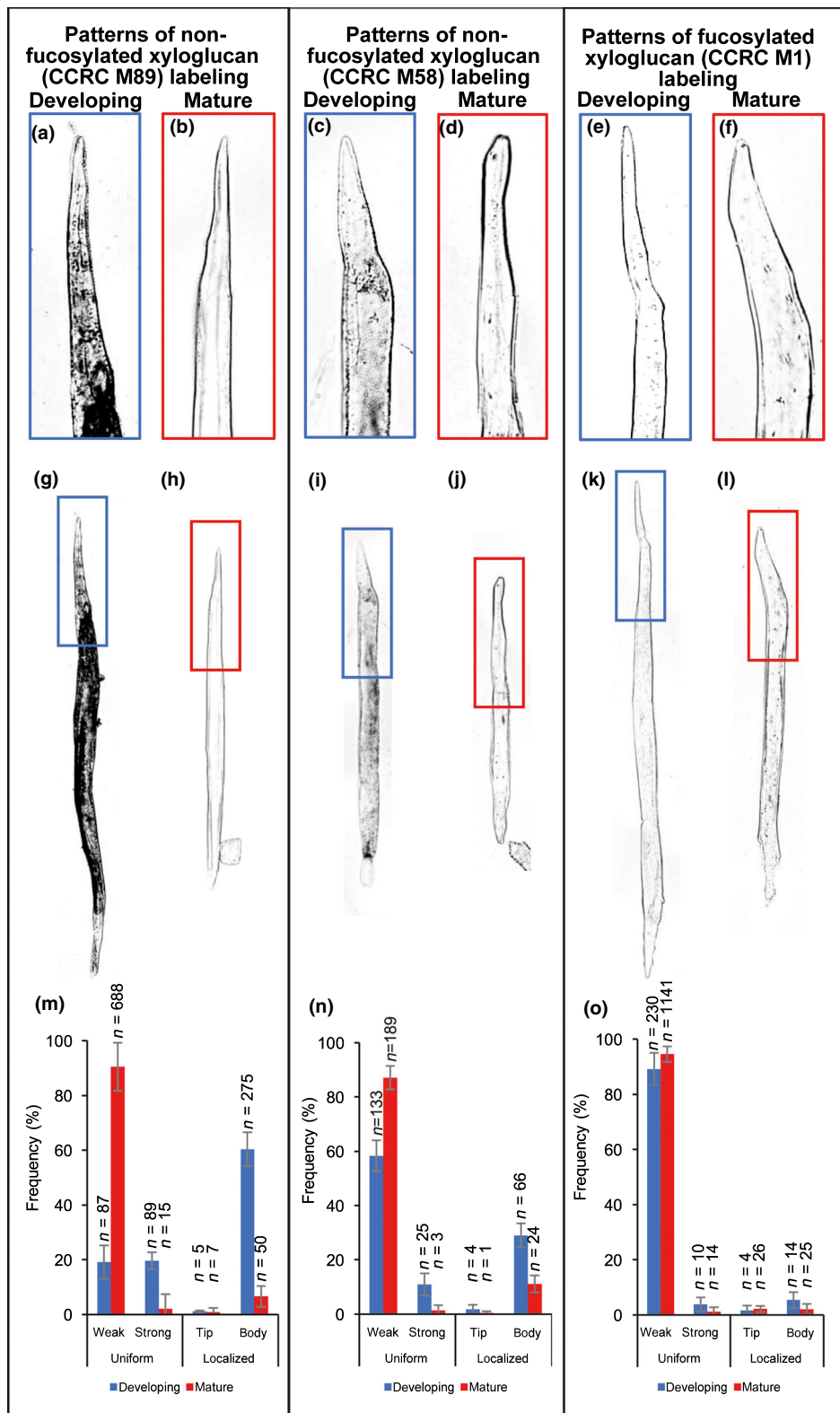
Fig. 5 Densities of nonfucosylated xyloglucan epitopes in developing fibers' cell walls are lowest at their tips. (a–l) Representative images of developing and mature fibers immunolabeled (as indicated by black signal) with monoclonal antibodies recognizing indicated epitopes of xyloglucan. The upper panel shows high-resolution images of tips of the fibers shown in the lower panel. Bars, 50 μm. (m–o) Graphs showing percentages of fibers with identified labeling patterns. Total numbers of analyzed fibers (n) are displayed on the bars. Data are means ± SE, calculated for independent immunolabeling experiments with developing and mature fibers (10 and eight experiments with CCRC-M89 antibodies, 10 and eight with CCRC-M58 antibodies, nine and nine with CCRC-M1 antibodies, respectively).
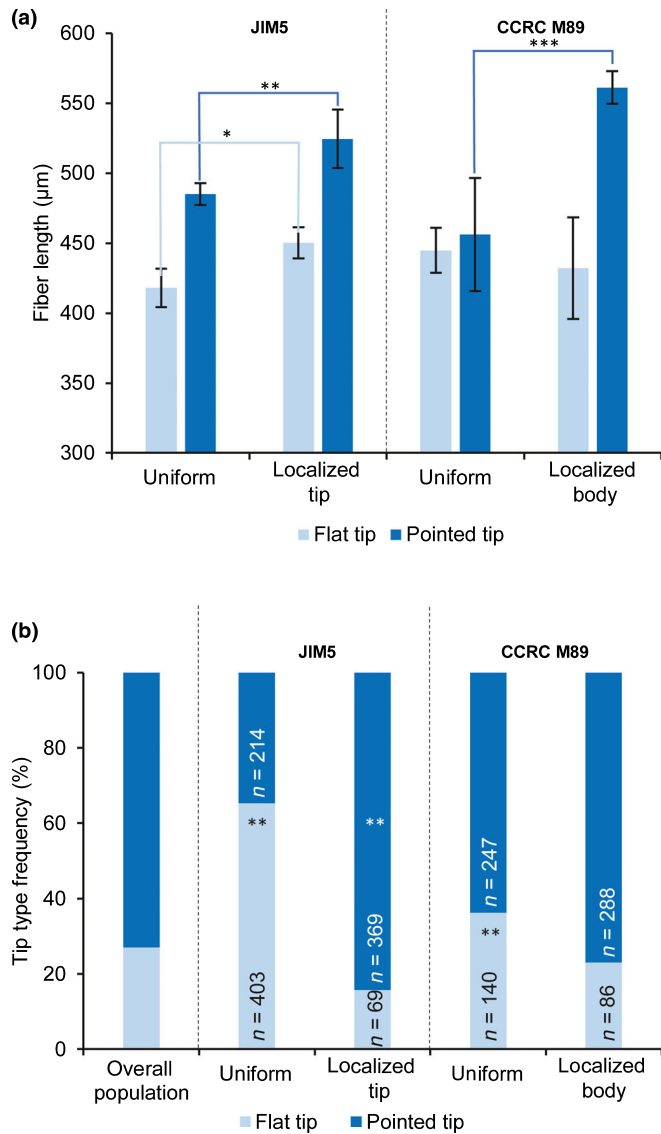
Fig. 6 Relationships between labeling patterns, lengths and tip shapes of developing fibers. (a) Lengths of fibers with localized and uniform labeling patters. Data are means ± SE, and the significance of differences according to *t*-tests is shown by asterisks (*, $P < 0.05$; **, $P < 0.01$; ***, $P < 0.001$). (b) Frequency distributions of flat and pointed tips assigned to each labeling category. *P*-values indicate the significance (according to the χ^2 test, $P < 0.01$) of the deviation of the frequencies of flat and pointed tips in each labeling category from the frequencies observed in the developing fiber population, estimated as 27% and 73% for flat and pointed tips, respectively.

intrusive growth must necessarily appear at junctions (Jura *et al.*, 2006). If a section of wall between cells away from a junction is separated, no space will open up at all. Furthermore, as the model shows that turgor pressure is the driving force that opens up the spaces, it is possible that unobserved spaces exist in sectioned and/or fixed tissue, which would open up if the sample could be visualized in its natural turgid state. In summary, the model shows that formation of the intercellular spaces involved in intrusive growth does not require any force from the intrusive cell, or growth to open up the spaces – only release of the middle lamella in a turgid tissue. This separation then causes the whole structure to expand in the radial direction, opening up room in both the radial and tangential directions for intruding tips.

Discussion

Xylem fibers have two distinct parts: bodies and extensions

The shape of mature xylem fibers determined by our AFM analysis (Figs 2, S3b) and three-dimensional (3D) reconstructions from serial transverse sections of wood (Fujiwara *et al.*, 1988; Yahya *et al.*, 2015) clearly allow distinction of the main body (the wide part with pit connections to adjacent cells) and the extensions (the narrower tapering parts, which are typically devoid of pits) (Larson, 1994; Chaffey *et al.*, 1999; Evert, 2006). The border between the body and extensions is sometimes marked by the presence of structures called 'knees' (Gorshkova *et al.*, 2012; Wilczek *et al.*, 2018). The length of the body corresponds to the length of xylem vessel elements and axial strands of parenchyma cells (Wenham & Cusick, 1975; Yahya *et al.*, 2015) that do not elongate during differentiation, and thus represents the length of xylem mother cells in the cambium (Larson, 1994; Mellerowicz, 2006). Fiber extensions terminate with pointed or flat tips. Flat shape is indicative of elongation being halted by an obstacle (Figs 1, 2, S3), for example a ray (Larson, 1994).

New cell wall is deposited over the entire surface of elongating xylem fibers

Fiber bodies have thicker walls than tips (Fig. 2), indicating that cell wall biosynthesis continues in entire fibers during their intrusive growth. The type of cell wall deposited in bodies of elongating fibers is currently unknown, but it probably resembles primary rather than secondary wall, as indicated by expression patterns of genes involved in primary and secondary wall formation (Sundell *et al.*, 2017). Moreover, the lignification of middle lamellae, which is concomitant with secondary wall formation (Mellerowicz *et al.*, 2001), would hinder formation of the intercellular spaces needed for fiber apical intrusion. Thickening of the entire wall of tip-growing cells has been previously observed. For example, a radiolabeled precursor was deposited in all parts of elongating root hairs (Wardrop, 1959). A distinct inner cell wall layer is deposited *c.* 10–50 µm behind the tip of root hairs and pollen tubes, which was interpreted as 'secondary' because various authors have observed no cell wall growth in that zone

Karczewska, 2009), because it would result in a higher tangential expansion of the cambial cylinder than observed. However, this idea does not take into account the effect of turgor after separation, which can harness displacement in the radial direction to provide room in the tangential direction for the intrusive tips to grow. Interestingly, the model suggests that tangential walls adjacent to the radial walls must be the ones primarily targeted for separation, as 10 times more of the tangential wall needs to be separated in order to obtain relatively isodiametrically shaped spaces. The model also explains why
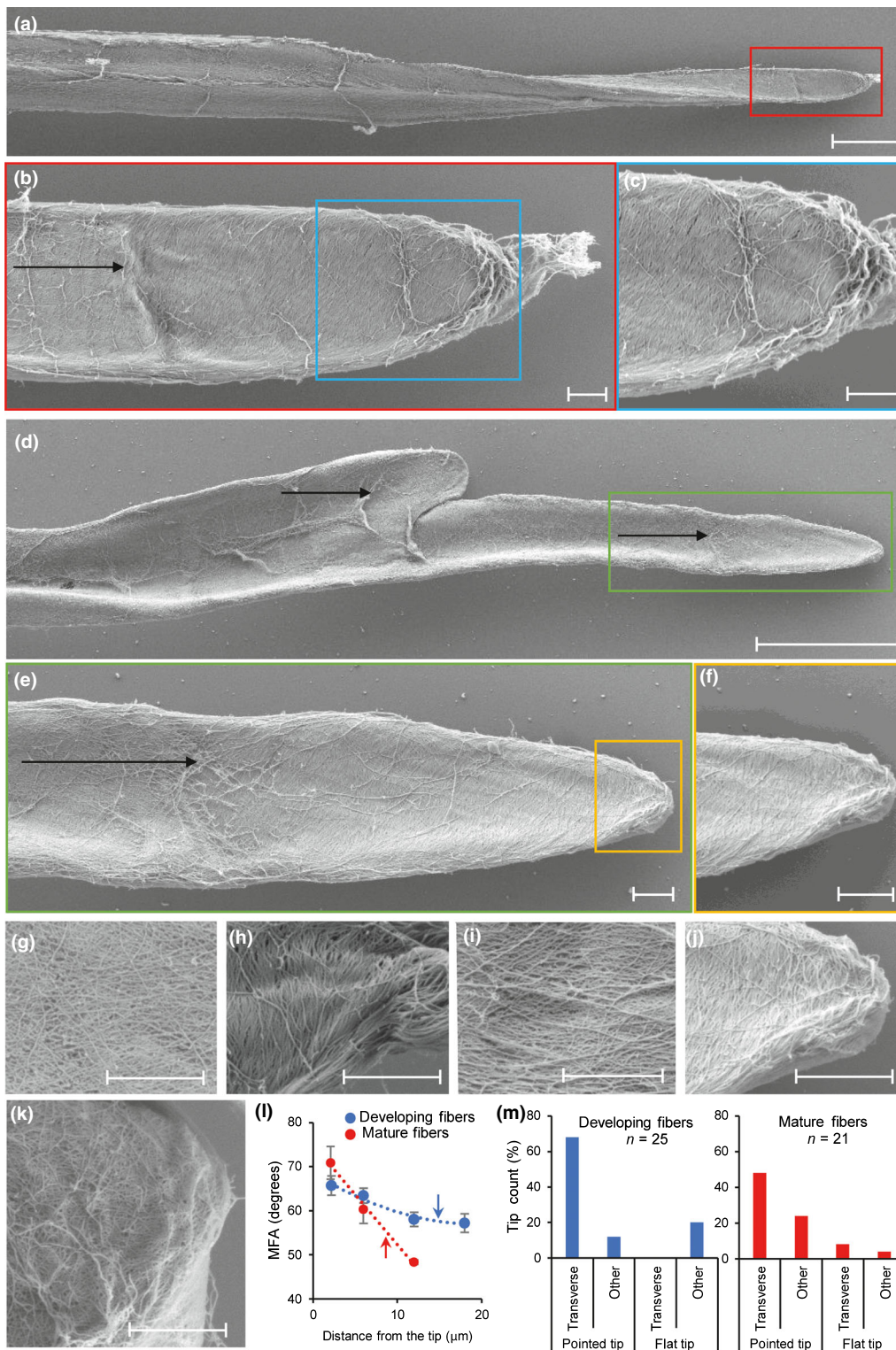
Fig. 7 Scanning electron microscopy images of developing and mature fibers showing differences in cell wall texture between their tips and bodies, and quantitative analysis of cellulose orientation. Representative images of a developing (a–c) and mature (d–f) fibers with pointed tips. Close-ups showing cell wall texture in developing (g–h) and mature (i–j) pointed tip fibers, their tips (h, j) and bodies (g, i), and in developing fibers with flat tips (k). Note the differences in cellulose microfibril orientation between pointed tips (c, f, h, j), flat tips (k) and the fiber bodies (b, e, g, i), and the discontinuous cell wall layer close to the growing tips (black arrows). The main axis of each fiber shown is in the horizontal plane. Bars: (a, d) 10 μm; (b, c, e–k)1 μm. (l, m) Numerical data showing microfibril angles (MFAs) in pointed tips of developing and mature fibers (l) and distribution of indicated types of cellulose microfibril orientations in each category of tips (m). The transverse category includes helicoidal, almost transverse orientation as shown in (c, h, j), whereas the other category includes longitudinal, cross-linked and disordered patterns, as shown in (g, i, k). Arrows in (l) show the mean distance from the tip to the transition in cell wall texture where the transverse MFA pattern was no longer visible. Data in (l) are means ± SE.
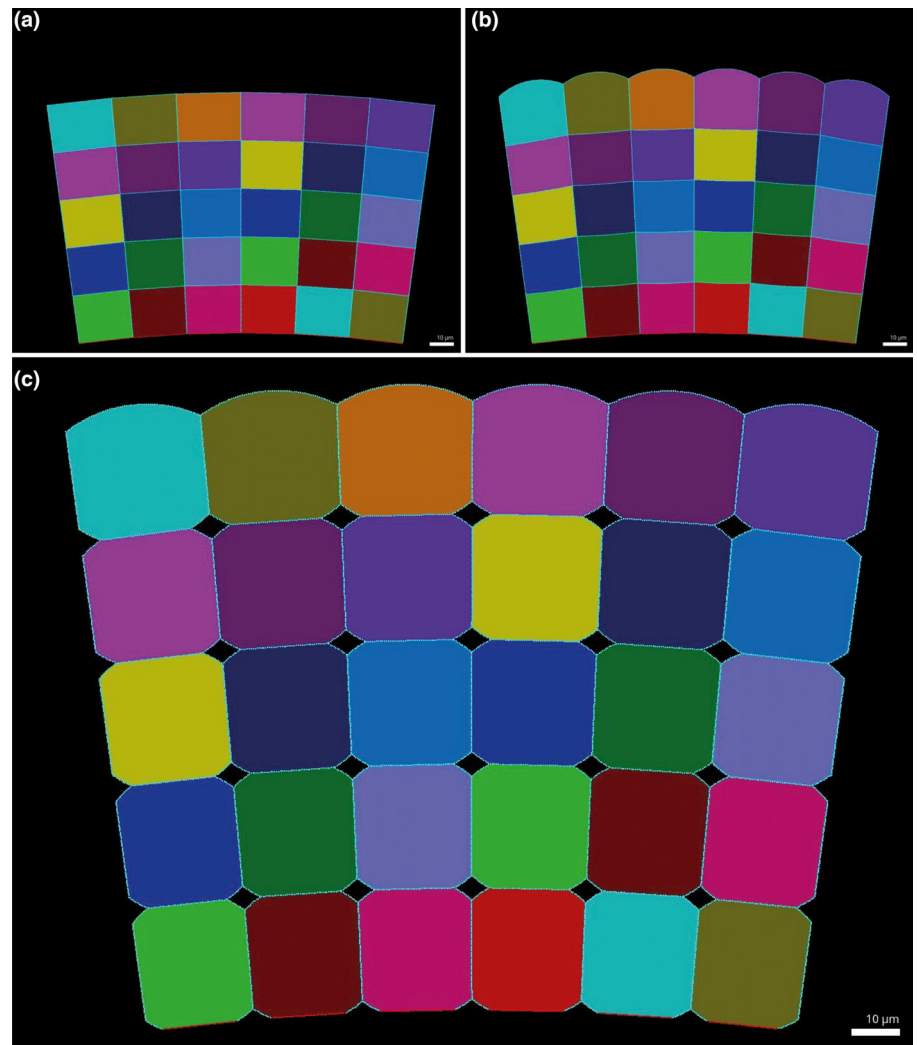
Fig. 8 Computational model of the turgor-induced formation of intercellular spaces in developing xylem. Trapezoidal cross-section of developing xylem tissue consisting of cells labeled with different colors. Cells are defined by vertices and edges (colored in cyan) that represent components in the mass-spring system. (a) Initially almost rectangular-shaped cells with no turgor pressure are connected by shared walls. (b) Turgor pressure induces expansion in the radial direction, as vertices on the sides do not allow lateral movement, simulating the presence of a full ring of tissue. Red vertices at the bottom are fixed in the vertical direction, simulating their attachment to the inner woody tissue. (c) The middle lamella is released by duplicating cell wall segments around the junctions. This causes intercellular spaces to appear as cells become rounder as a result of turgor pressure, providing space for the intrusive growth of fiber tips.

(Ferguson *et al.*, 1998; Emons & Wolters-Art, 1983; Akkerman *et al.*, 2012; Lampugnani *et al.*, 2013). However, it is not known if its matrix composition corresponds to that of secondary wall, or if enzymes responsible for secondary wall biosynthesis are involved.

In later stages of development, xylem fibers deposit typical secondary wall layer material over the entire cell wall surface, including bodies and extensions with tips, and all wall layers become lignified (Fig. 1). However, the cell wall thickness of the tips remains two times smaller compared with bodies (Fig. 2). Moreover, the thickness of the bodies' wall is uneven, peaking in the middle and gradually declining towards the extensions. A similar gradual decrease in wall thickness has been detected in mature xylem fibers of *Acacia magium* by 3D reconstruction of serial sections (Yahya *et al.*, 2015). These observations suggest that secondary wall deposition is adjusted in response to perceived local signals (Derba-Maceluch *et al.*, 2015; Ratke *et al.*, 2018) that presumably optimize the tissue's mechanical strength. Secondary wall is also deposited in phloem fibers, but in even thickness (Ageeva *et al.*, 2005; Snegireva *et al.*, 2010, 2015).

Intrusive apical elongation is accompanied by transverse cellulose microfibril orientation

Scanning electron microscopy analysis of elongating xylem fibers revealed that their tips have an ordered transverse cellulose arrangement, which changes to a flat helical, S-type arrangement within < 20 µm of the apex, followed by a change in cell wall texture indicative of cross-linking and maturation (Fig. 7). This type of arrangement of cellulose microfibrils suggests that cell wall expansion might be limited to the short subapical region of the fiber extensions; however, the orientation of cellulose in the inner cell wall layers should be studied to confirm this hypothesis. This hypothesis agrees with the previous reports of steep helicoidal microtubules in elongating fibers (Chaffey *et al.*, 1997, 1999), which precludes their overall elongation. Transverse cortical microtubules indicative of transverse cellulose microfibrils have been reported in elongating cotton (Yu *et al.*, 2019) and phloem (Ageeva *et al.*, 2005) fibers, whereas neither cellulose nor microtubules had this kind of orientation at the tips of pollen tubes or root hairs (Emons & Wolters-Arts, 1983; Ferguson *et al.*, 1998;

Akkerman *et al.*, 2012; Chebli *et al.*, 2012; Bidhendi *et al.*, 2020), indicating a fundamental difference in the modes of elongation of these two groups of cells. Transverse orientation of cellulose microfibrils allows elongation by diffusive growth, which causes microfibril reorientation to a helical pattern (Anderson *et al.*, 2010). Therefore, xylem fibers could exhibit some diffuse elongation of the subapical region.

Apical intrusive growth of xylem fibers is associated with tip-oriented distributions of partially de-esterified HG epitopes

Immunolabeling indicated that partially de-esterified HG epitopes accumulate within the primary wall layer at the tips of actively elongating xylem fibers (Figs 3, 4, 6, S7, S8). This pattern could be caused by specific deposition of HG and/or its de-esterification at the tips, although epitope masking in the older regions of fiber wall cannot be excluded. The viscoelastic properties of cell walls, and hence wall elongation, are known to correlate with HG high/low methylesterified epitope distribution and HG esterification status in plants and algae (Eder & Lütz-Meindl, 2008; Palin & Geitmann, 2012; Boyer, 2016; Phyo *et al.*, 2017). Heterogeneous distributions of de-esterified HG precede a switch from isotropic to anisotropic growth with reorganization of cellulose deposition (Peaucelle *et al.*, 2011, 2015). In pollen tubes, there is a characteristic sharp boundary between highly methylesterified and de-esterified HG controlled by secretion of pectin methylesterases (PMEs) and PME inhibitors (Li *et al.*, 1994; Bosch *et al.*, 2005; Parre & Geitmann, 2005; Rojas *et al.*, 2011), whereas in root hairs, the content of HG is high but no change in esterification has been detected (Mravec *et al.*, 2017). Ca^{2+} binding to de-esterified stretches of HG can stiffen the walls (Ezaki *et al.*, 2005), leading to growth inhibition, which has been observed following ectopic overexpression of *AtPME1* in *Arabidopsis* (Derbyshire *et al.*, 2007) and *PtxtPME1* in aspen (Siedlecka *et al.*, 2008). However, local HG de-esterification is thought to facilitate its degradation by polygalacturonases and pectate lyases, which weakens walls (Parre & Geitmann, 2005). De-esterification of HG in the subapical region of elongating fibers could have a role in strengthening the wall during or following expansion (Siedlecka *et al.*, 2008) and/or mediating the direction of cellulose biosynthesis (Peaucelle *et al.*, 2015).

Polarized distributions of XG epitopes in xylem fibers suggest a role in apical intrusive elongation

We detected strong accumulation of nonfucosylated XG epitopes in fiber bodies, but only weak and uniform distribution of fucosylated XG epitopes (Figs 5, 6, S7). Detection of XG epitopes could be affected by the fiber isolation procedure, because in chemically fixed tissue CCRC-M1 epitopes are abundant (Bourquin *et al.*, 2002; Nishikubo *et al.*, 2011). Nevertheless, the results corroborate the polarization of XG epitopes in elongating fibers between their bodies and extensions, reflecting either the epitope abundance or masking. The

polarity supports the differential expansion of fiber extensions and bodies. Indeed, XG metabolism by xyloglucan endotransglycosylase (XET) has been shown to affect xylem fiber elongation (Nishikubo *et al.*, 2011; Kushwah *et al.*, 2020). This is consistent with known involvement of XG in polar growth in other tissues (Hayashi, 1989; Takeda *et al.*, 2002; Cavalier *et al.*, 2008; Majda *et al.*, 2017). Root hair elongation in *Arabidopsis* requires GlcA substitution of XG (Peña *et al.*, 2012). Xyloglucan and XET activity are concentrated at root hair tips (Vissenberg *et al.*, 2001; Cavalier *et al.*, 2008; Larson *et al.*, 2014) and plants grown in the presence of XETs (Maris *et al.*, 2009) and mutants defective in XG biosynthesis (Cavalier *et al.*, 2008; Zabotina *et al.*, 2008, 2012; Wang *et al.*, 2014) develop bulging in proximal parts of root hairs, indicating that XG is essential for strengthening their cell walls. Taken together, these data indicate that XG structure and metabolism are involved in the elongation of cell walls in various types of tip-growing cells.

Intercellular spaces required for fibers' intrusive apical elongation can be formed solely by release of the middle lamella

Early microscopy studies showed that xylem fibers grow between adjacent cells, but the mechanism involved in the cells' separation at their joint middle lamella remained a matter of speculation (Wenham & Cusick, 1975; Gorshkova *et al.*, 2012). Our computer simulations showed that turgor pressure alone is enough to induce the formation of intercellular spaces at cell junctions if the middle lamella is released (Fig. 8), thereby creating spaces for nearby fiber tips to invade. A similar process could underlie cell separation in other tissues (Jarvis, 1998; Zhang *et al.*, 2020). This finding shows that there is no need for mechanical pressure from the tips to make room for intrusive growth, confirming earlier hypotheses by Wenham & Cusick (1975) that were postulated based on the geometry of elongating fibers. The formation of intercellular spaces could potentially be assisted by the secretion of enzymes that digest the middle lamellae by the growing fiber tips themselves or the neighboring fibers. In either case, cell separation would be locally induced, enabling intrusive growth and establishment of new cell contacts, and cell adhesion involving new partners. More studies are required to elucidate the process further.

Proposed model of xylem fiber intrusive elongation

Considering previously published data and results presented here, we propose that intrusive apical growth of differentiating wood fibers (Fig. 9) is initiated by the formation of intercellular space and establishment of a 'knee' characterized by localized deposition and de-esterification of HG. As a result, as suggested by the recent work of Peaucelle *et al.* (2015), the cortical microtubules change their orientation and cellulose deposition becomes highly ordered and almost transverse close to the apex, which allows tip axis elongation that induces stretching of the microfibrils to a steeper helical orientation.
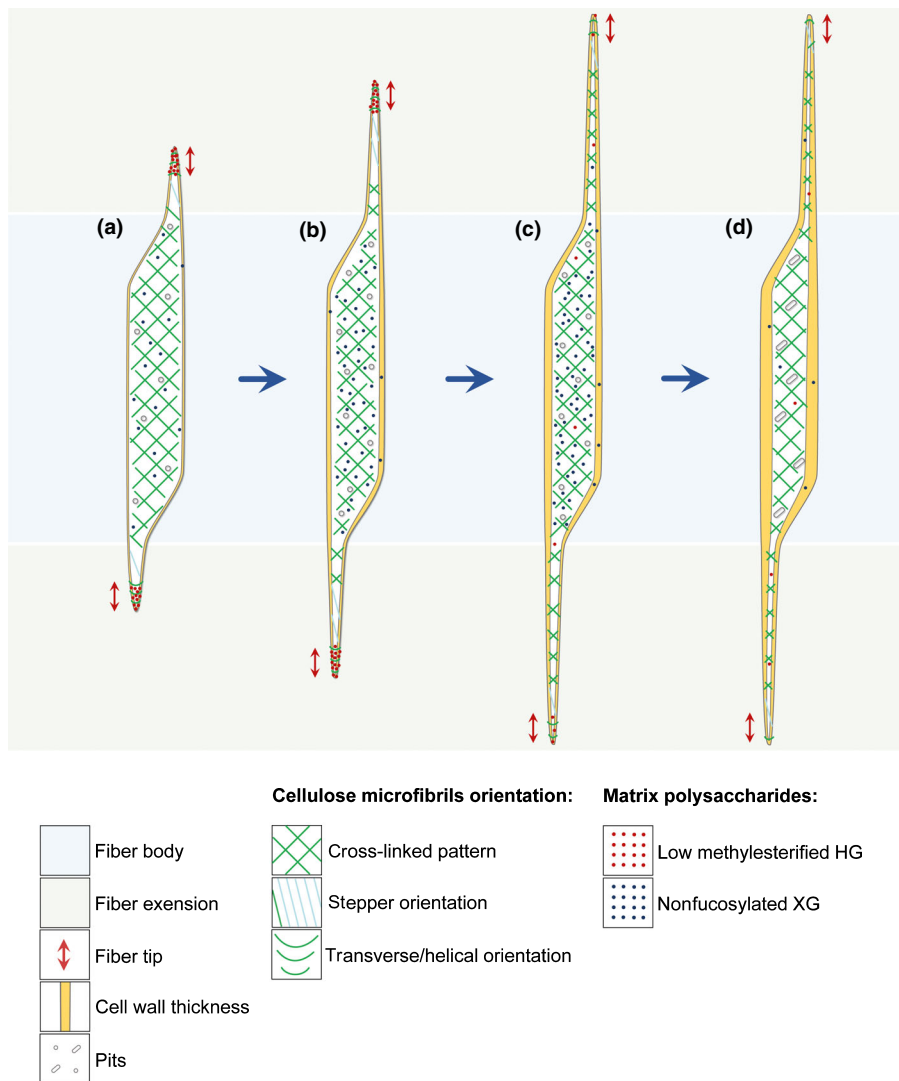
Cellulose microfibrils orientation:

Cross-linked pattern

Stepper orientation

Transverse/helical orientation

Matrix polysaccharides:

Low methylesterified HG

Nonfucosylated XG

Fiber body

Fiber exension

Fiber tip

Cell wall thickness

Pits

Fig. 9 Summary of findings regarding xylem fibers' elongation by apical intrusive growth and proposed mechanism of apical elongation. Diagrams show four stages of fiber differentiation: (a) initiation of elongation, (b) active elongation, (c) end of elongation, and (d) mature stage after secondary wall deposition. We propose that growth is initiated by localized secretion of middle lamella-digesting enzymes (pectin methylesterases, polygalacturonases and pectate lyases) causing the release of cell adhesion. The mechanical simulation shows that the release of cell adhesion in turgid cells drives the formation of intercellular spaces between the fibers at the junctions. The tips stimulated by an unknown trigger start growing into these spaces. Their growth involves the deposition of homogalacturonans (HGs) followed by their partial de-esterification (as can be deduced from immunolabeling experiments), initially at the cell corner (a), and subsequently at a resulting growing tip (b), which is detectable early in the cambium/radial expansion zone. This is accompanied by the reorganization of cellulose biosynthesis, leading to the deposition of microfibrils in a highly ordered transverse orientation in the subapical region, as seen in scanning electron microscopy (SEM). This allows the subapical elongation with stretching of cellulose microfibrils into a steeper helix recorded in SEM images. The elongation is followed by cellulose cross-linking in the outer cell wall layers, with participation of nonfucosylated xyloglucans (XGs), as indicated by immunolabeling experiments, as shown in (b) and (c). Deposition of the wall continues over the entire surface of the fiber during its elongation, leading to a thicker wall in the body than at the tips, as recorded by atomic force microscopy. Following fiber elongation, secondary S1 and S2 wall layers are deposited with the thickest S2 layer having helical Z-type microfibril angle as illustrated by the shape pits, and the entire fiber becomes lignified with disappearance of polar distribution of HG and nonfucosylated XG epitopes, as revealed by immunolabeling, which could be caused by masking by lignin or by other factors.

The growth of the subapical part might be halted by cellulose cross-linking and stiffening of the cell walls with participation of XG. The wall continues to be deposited over the entire surface of the fibers, including the bodies, which are not elongating and have substantial pit connections with radially adjacent cells. Following elongation, the secondary S1 and S2 (and sometimes S3) cell wall layers are deposited over the entire cell wall surface, with distinct altering of the orientation of cellulose microfibril helixes, as evident from changes in cortical microtubules documented by Chaffey *et al.* (1997, 1999); all wall layers lignify and the fibers undergo programmed cell death (Courtois-Moreau *et al.*, 2009). This mode of elongation of xylem fibers is distinct, despite some similarities with elongation of pollen tubes, root hairs and phloem fibers.

New
Phytologist

Acknowledgements

Author contributions

MM, LK, AB and EJM designed the research. MM developed and applied protocols for the immunolocalization analyses of macerated fibers (by LM and SEM) and ultrathin sections (by TEM), and then analyzed the data with help of AB and MD-M. IAI and LK developed AFM procedures for isolated fibers. LK and TG carried out AFM analyses. LAM-R secured the funding and supervised the AFM work. LK performed SEM cellulose analyses. RSS developed the computer model. MM and EJM wrote the manuscript with contributions from all co-authors.

ORCID

Alicja Banasiak (iD) https://orcid.org/0000-0003-4293-8948
Marta Derba-Maceluch (iD) https://orcid.org/0000-0002-8034-3630
Tatyana Gorshkova (iD) https://orcid.org/0000-0003-0342-8195
Igor A. Iashchishyn (iD) https://orcid.org/0000-0002-1691-9025
Liudmila Kozlova (iD) https://orcid.org/0000-0002-6323-167X
Mateusz Majda (iD) https://orcid.org/0000-0003-3405-2901
Ewa J. Mellerowicz (iD) https://orcid.org/0000-0001-6817-1031
Ludmilla A. Morozova-Roche (iD) https://orcid.org/0000-0001-5886-2023
Richard S. Smith (iD) https://orcid.org/0000-0001-9220-0787

References

Ageeva MV, Petrovská B, Kieft H, Sal'nikov VV, Snegireva AV, van Dam JEG, van Veenendaal WLH, Emons AMC, Gorshkova TA, van Lammeren AAM. 2005. Intrusive growth of flax phloem fibers is of intercalary type. *Planta* **222**: 565–574.

Akkerman M, Franssen-Verheijen M, Immerzeel P, Hollander L, Schel J, Emons A. 2012. Texture of cellulose microfibrils of root hair cell walls of *Arabidopsis thaliana, Medicago truncatula*, and *Vicia sativa*. *Journal of Microscopy* **247**: 60–67.

Andersen M, Boos I, Marcus S, Kračun S, Rydahl M, Willats W, Knox J, Clausen M. 2016. Characterization of the LM5 pectic galactan epitope with synthetic analogues of β-1,4-D-galactotetraose. *Carbohydrate Research* **436**: 36–40.

Anderson CT, Carroll A, Akhmetova L, Somerville C. 2010. Real-time imaging of cellulose reorientation during cell wall expansion in *Arabidopsis* roots. *Plant Physiology* **152**: 787–796.

Bidhendi AJ, Chebli Y, Geitmann A. 2020. Fluorescence visualization of cellulose and pectin in the primary plant cell wall. *Journal of Microscopy* **278**: 164–181.

Bosch M, Cheung AY, Hepler PK. 2005. Pectin methylesterase, a regulator of pollen tube growth. *Plant Physiology* **138**: 1334–1346.

Bourquin V, Nishikubo N, Abe H, Brumer H, Denman S, Eklund M, Christiernin M, Teeri TT, Sundberg B, Mellerowicz EJ. 2002. Xyloglucan endotransglycosylases have a function during the formation of secondary cell walls of vascular tissues. *Plant Cell* **14**: 3073–3088.

Boyer JS. 2016. Enzyme-less growth in *Chara* and terrestrial plants. *Frontiers in Plant Science* **7**: 866.

Cavalier DM, Lerouxel O, Neumetzler L, Yamauchi K, Reinecke A, Freshour G, Zabotina OA, Hahn MG, Burgert I, Pauly M et al. 2008. Disrupting two *Arabidopsis thaliana* xylosyltransferase genes results in plants deficient in xyloglucan, a major primary cell wall component. *Plant Cell* **20**: 1519–1537.

Chaffey N, Barlow P, Barnett J. 1997. Cortical microtubules rearrange during differentiation of vascular cambial derivatives, microfilaments do not. *Trees* **11**: 333–341.

Chaffey N, Barnett J, Barlow P. 1999. A cytoskeletal basis for wood formation in angiosperm trees: the involvement of cortical microtubules. *Planta* **208**: 19–30.

Chebli Y, Kaneda M, Zerzour R, Geitmann A. 2012. The cell wall of the *Arabidopsis* pollen tube - spatial distribution, recycling, and network formation of polysaccharides. *Plant Physiology* **160**: 1940–1955.

Cheung AY. 1996. Pollen-pistil interactions during pollen-tube growth. *Trends in Plant Science* **1**: 45–51.

Clausen M, Willats W, Knox J. 2003. Synthetic methyl hexagalacturonate hapten inhibitors of anti-homogalacturonan monoclonal antibodies LM7, JIM5 and JIM7. *Carbohydrate Research* **338**: 1797–1800.

Courtois-Moreau CL, Pesquet E, Sjödin A, Muniz L, Bollhöner B, Kaneda M, Samuels L, Jansson S, Tuominen H. 2009. A unique program for cell death in xylem fibers of *Populus* stem. *The Plant Journal* **58**: 260–274.

Derba-Maceluch M, Awano T, Takahashi J, Lucenius J, Ratke C, Kontro I, Busse-Wicher M, Kosik O, Tanaka R, Winzéll A et al. 2015. Suppression of xylan endotransglycosylase PtxtXyn10A affects cellulose microfibril angle in secondary wall in aspen wood. *New Phytologist* **205**: 666–681.

Derbyshire P, McCann MC, Roberts K. 2007. Restricted cell elongation in *Arabidopsis* hypocotyls is associated with a reduced average pectin esterification level. *BMC Plant Biology* **7**: 1–12.

Eder M, Lütz-Meindl U. 2008. Pectin-like carbohydrates in the green alga *Micrasterias* characterized by cytochemical analysis and energy filtering TEM. *Journal of Microscopy* **231**: 201–214.

Emons AMC, Wolters-Arts A. 1983. Cortical microtubules and microfibril deposition in the cell wall of root hairs of *Equisetum hyemale*. *Protoplasma* **81**: 68–81.

Esau K. 1943. Vascular differentiation in the vegetative shoot of *Linum*: 3. The origin of bast fibers. *American Journal of Botany* **30**: 579–586.

Esau K. 1953. *Plant anatomy.* New York, NY, USA: John Wiley & Sons.

Evert RF. 2006. *Esau's plant anatomy, 3rd edn.* Hoboken, NJ, USA: John Wiley & Sons.

Ezaki N, Kido N, Takahashi K, Katou K. 2005. The role of wall Ca^{2+} in the regulation of wall extensibility during the acid-induced extension of soybean hypocotyl cell walls. *Plant and Cell Physiology* **46**: 1831–1838.

Ferguson C, Teeri TT, Siika-aho M, Read SM, Bacic A. 1998. Location of cellulose and callose in pollen tubes and grains of *Nicotiana tabacum*. *Planta* **206**: 452–460.

Fujiwara T, Saiki H, Fujita M. 1988. Stereo-analysis of morphology of hardwood fibers with serial transverse sections. *Bull Kyoto Univ For* **60**: 269–275.

Gendreau E, Traas J, Desnos T, Grandjean O, Caboche M, Höfte H. 1997. Cellular basis of hypocotyl growth in *Arabidopsis thaliana*. *Plant Physiology* **114**: 295–305.

Gorshkova T, Brutch N, Chabbert B, Deyholos M HT, Lev-Yadun S, Mellerowicz EJ, Morvan C, Neutelings G, Pilate G. 2012. Plant fiber

formation: state of the art, recent and expected progress, and open questions. *Critical Reviews in Plant Sciences* **31**: 201–228.

Gorshkova T, Chernova T, Mokshina N, Gorshkov V, Kozlova L, Gorshkov O. 2018. Transcriptome analysis of intrusively growing flax fibers isolated by laser microdissection. *Scientific Reports* **8**: 14570.

Gorshkova TA, Salnikov VV, Chemikosova SB, Ageeva MV, Pavlencheva NV, Van Dam JEG. 2003. The snap point: a transition point in *Linum usitatissimum* bast fiber development. *Industrial Crops and Products* **18**: 213–221.

Gray-Mitsumune M, Blomquist K, McQueen-Mason S, Teeri TT, Sundberg B, Mellerowicz EJ. 2008. Ectopic expression of a wood-abundant expansin PttEXPA1 promotes cell expansion in primary and secondary tissues in aspen. *Plant Biotechnology Journal* **6**: 62–72.

Gray-Mitsumune M, Mellerowicz EJ, Abe H, Schrader J, Winzéll A, Sterky F, Blomqvist K, McQueen-Mason S, Teeri TT, Sundberg B. 2004. Expansins abundant in secondary xylem belong to subgroup A of the alpha-expansin gene family. *Plant Physiology* **135**: 1552–1564.

Green PB. 1962. Mechanism for plant cellular morphogenesis. *Science* **138**: 1404–1405.

Gu F, Nielsen E. 2013. Targeting and regulation of cell wall synthesis during tip growth in plants. *Journal of Integrative Plant Biology* **55**: 835–846.

Guedes FTP, Laurans F, Quemener B, Assor C, Lainé-Prade V, Boizot N, Vigouroux J, Lesage-Descauses M-C, Leplé J-C, Déjardin A et al. 2017. Non-cellulosic polysaccharide distribution during G-layer formation in poplar tension wood fibers: abundance of rhamnogalacturonan I and arabinogalactan proteins but no evidence of xyloglucan. *Planta* **246**: 857–878.

Guerriero G, Hausman JF, Cai G. 2014. No stress! Relax! Mechanisms governing growth and shape in plant cells. *International Journal of Molecular Sciences* **15**: 5094–5114.

Guimil S, Dunand C. 2007. Cell growth and differentiation in *Arabidopsis* epidermal cells. *Journal of Experimental Botany* **58**: 3829–3840.

Hayashi T. 1989. Xyloglucans in the primary cell wall. *Annual Review of Plant Physiology and Plant Molecular Biology* **40**: 139–168.

Jarvis MC. 1998. Intercellular separation forces generated by intracellular pressure. *Plant, Cell & Environment* **21**: 1307–1310.

Jura J, Kojs P, Iqbal M, Szymanowska-Pułka J, Włoch W. 2006. Apical intrusive growth of cambial fusiform initials along the tangential walls of adjacent fusiform initials: evidence for a new concept. *Australian Journal of Botany* **54**: 493.

Karczewska A. 2009. Regularity of solutions to stochastic Volterra equations of convolution type. *Integral Transforms and Special Functions* **20**: 171–176.

Kasili R, Huang CC, Walker JD, Simmons LA, Zhou J, Faulk C, Hulskamp M, Larkin JC. 2011. BRANCHLESS TRICHOMES links cell shape and cell cycle control in *Arabidopsis* trichomes. *Development* **138**: 2379–2388.

Knox JP, Linstead PJ, King JJ, Cooper C, Roberts K. 1990. Pectin esterification is spatially regulated both within cell walls and between developing tissues of root apices. *Planta* **181**: 512–521.

Kushwah S, Banasiak A, Nishikubo N, Derba-Maceluch M, Majda M, Endo S, Kumar V, Gomez L, Gorzsás A, McQueen-Mason S et al. 2020. Arabidopsis XTH4 and XTH9 contribute to wood cell expansion and secondary wall formation. *Plant Physiology* **182**: 1946–1965.

Lampugnani ER, Moller IE, Cassin A, Jones DF, Koh PL, Ratnayake S, Beahan CT, Wilson SM, Bacic A, Newbigin E. 2013. *In vitro* grown pollen tubes of *Nicotiana alata* actively synthesise a fucosylated xyloglucan. *PLoS ONE* **8**: e77140.

Larson ER, Tierney MR, Tinaz B, Domozych DS. 2014. Using monoclonal antibodies to label living root hairs: a novel tool for studying cell wall microarchitecture and dynamics in *Arabidopsis. Plant Methods* **10**: 30.

Larson PR. 1994. *The vascular cambium.* Berlin, Germany: Springer Series in Wood Science, Springer-Verlag.

Lee K, Sakata Y, Mau S, Pettolino F, Bacic A, Quatrano R, Knight C, Knox J. 2005. Arabinogalactan proteins are required for apical cell extension in the moss *Physcomitrella patens. Plant Cell* **17**: 3051–3065.

Lev-Yadun S. 2001. Intrusive growth – the plant analog of dendrite and axon growth in animals. *New Phytologist* **150**: 508–512.

Li YQ, Chen F, Linskens HF, Cresti M. 1994. Distribution of unesterified and esterified pectins in cell walls of pollen tubes of flowering plants. *Sexual Plant Reproduction* **7**: 145–152.

Majda M. 2019. Visualization of plant cell wall epitopes using immunogold labeling for electron microscopy. *Bio-protocol* **9**: e3205.

Majda M, Grones P, Sintorn I-M, Vain T, Milani P, Krupinski P, Zagórska-Marek B, Viotti C, Jönsson H, Mellerowicz EJ et al. 2017. Mechanochemical polarization of contiguous cell walls shapes plant pavement cells. *Developmental Cell* **43**: 290–304.e4.

Marcus SE, Blake AW, Benians TAS, Lee KJD, Poyser C, Donaldson L, Leroux O, Rogowski A, Petersen HL, Boraston A et al. 2010. Restricted access of proteins to mannan polysaccharides in intact plant cell walls. *The Plant Journal* **64**: 191–203.

Maris A, Suslov D, Fry SC, Verbelen JP, Vissenberg K. 2009. Enzymic characterization of two recombinant xyloglucan endotransglucosylase/hydrolase (XTH) proteins of *Arabidopsis* and their effect on root growth and cell wall extension. *Journal of Experimental Botany* **60**: 3959–3972.

Mathur J. 2004. Cell shape development in plants. *Trends in Plant Science* **9**: 583–590.

McCartney L, Marcus SE, Knox JP. 2005. Monoclonal antibodies to plant cell wall xylans and arabinoxylans. *Journal of Histochemistry and Cytochemistry* **53**: 543–546.

Mellerowicz EJ. 2006. Xylem cell expansion – lessons from poplar. In: Hayashi T, ed. *The science and lore of the plant cell wall.* Boca Raton, FL, USA: Universal Publishers Brown Walker Press, 267–275.

Mellerowicz EJ, Baucher M, Sundberg B, Bojeran W. 2001. Unraveling cell wall formation in the woody dicot stem. *Plant Molecular Biology* **47**: 239–274.

Mellerowicz EJ, Gorshkova T. 2012. Tensional stress generation in gelatinous fibres: a review and possible mechanism based on cell wall structure and composition. *Journal of Experimental Botany* **63**: 551–565.

Mosca G, Adibi M, Strauss S, Runions A, Sapala A, Smith RS. 2018. Modeling plant tissue growth and cell division. In: Morris RJ, ed. *Mathematical modelling in plant biology.* Cham, Switzerland: Springer, 107–138.

Mosca G, Sapala A, Strauss S, Routier-Kierzkowska AL, Smith RS. 2017. On the micro-indentation of plant cells in a tissue context. *Physical Biology* **14**: 15003.

Mravec J, Kracun SK, Rydahl MG, Westereng B, Pontiggia D, De Lorenzo G, Domozych DS, Willats WGT. 2017. An oligogalacturonide-derived molecular probe demonstrates the dynamics of calcium-mediated pectin complexation in cell walls of tip-growing structures. *The Plant Journal* **91**: 534–546.

Nishikubo N, Takahashi J, Roos AA, Derba-Maceluch M, Piens K, Brumer H, Teeri TT, Stålbrand H, Mellerowicz EJ. 2011. Xyloglucan endo-transglycosylase-mediated xyloglucan rearrangements in developing wood of hybrid aspen. *Plant Physiology* **155**: 399–413.

Palin R, Geitmann A. 2012. The role of pectin in plant morphogenesis. *BioSystems* **109**: 397–402.

Park S, Szumlanski AL, Gu F, Guo F, Nielsen E. 2011. A role for CSLD3 during cell-wall synthesis in apical plasma membranes of tip growing root-hair cells. *Nature Cell Biology* **13**: 973–980.

Parker JS, Cavell AC, Dolan L, Roberts K, Grierson CS. 2000. Genetic interactions during root hair morphogenesis in *Arabidopsis. Plant Cell* **12**: 1961–1974.

Parre E, Geitmann A. 2005. Pectin and the role of the physical properties of the cell wall in pollen tube growth of *Solanum chacoense. Planta* **220**: 582–592.

Pattathil S, Avci U, Baldwin D, Swennes A, McGill J, Popper Z, Bootten T, Albert A, Davis R, Chennareddy C et al. 2010. Comprehensive toolkit of plant cell wall glycan-directed monoclonal antibodies. *Plant Physiology* **153**: 514–525.

Peaucelle A, Braybrook SA, Le Guillou L, Bron E, Kuhlemeier C, Höfte H. 2011. Pectin induced changes in cell wall mechanics underlie organ initiation in *Arabidopsis. Current Biology* **21**: 1720–1726.

Peaucelle A, Wightman R, Höfte H. 2015. The control of growth symmetry breaking in the Arabidopsis hypocotyl. *Current Biology* **25**: 1746–1752.

Pedersen HL, Fangel JU, McCleary B, Ruzanski C, Rydahl MG, Ralet M-C, Farkas V, von Schantz L, Marcus SE, Andersen MCF *et al.* 2012. Versatile high resolution oligosaccharide microarrays for plant glycobiology and cell wall research. *Journal of Biological Chemistry* 287: 39429–39438.

Peña MJ, Kong Y, York WS, O'Neill MA. 2012. A galacturonic acid-containing xyloglucan is involved in *Arabidopsis* root hair tip growth. *Plant Cell* 24: 4511–4524.

Phyo P, Wang T, Kiemle SN, O'Neill H, Pingali SV, Hong M, Cosgrove DJ. 2017. Gradients in wall mechanics and polysaccharides along growing inflorescence stems. *Plant Physiology* 175: 1593–1607.

Priestley JH. 1930. Studies in the physiology of cambial activity: II. The concept of sliding growth. *New Phytologist* 29: 96–140.

Ratke C, Terebieniec BK, Winestrand S, Derba-Maceluch M, Grahn T, Schiffthaler B, Ulvcrona T, Özparpucu M, Rüggeberg M, Lundqvist SO *et al.* 2018. Downregulating aspen xylan biosynthetic GT43 genes in developing wood stimulates growth via reprograming of transcriptome. *New Phytologist* 219: 230–245.

Roach MJ, Deyholos MK. 2008. Microarray analysis of developing flax hypocotyls identifies novel transcripts correlated with specific stages of phloem fibre differentiation. *Annals of Botany* 102: 317–330.

Rojas ER, Hotton S, Dumais J. 2011. Chemically mediated mechanical expansion of the pollen tube cell wall. *Biophysical Journal* 101: 1844–1853.

Ruprecht C, Bartetzko MP, Senf D, Dallabernadina P, Boos I, Andersen MCF, Kotake T, Knox JP, Hahn MG, Clausen MH *et al.* 2017. A synthetic glycan microarray enables epitope mapping of plant cell wall glycan-directed antibodies. *Plant Physiology* 175: 1094–1104.

Scheller HV, Ulvskov P. 2010. Hemicelluloses. *Annual Review of Plant Biology* 61: 263–289.

Schiefelbein JW, Somerville C. 1990. Genetic control of root hair development in *Arabidopsis thaliana*. *Plant Cell* 2: 235–243.

Siedlecka A, Wiklund S, Péronne MA, Micheli F, Lesniewska J, Sethson I, Edlund U, Richard L, Sundberg B, Mellerowicz EJ. 2008. Pectin methyl esterase inhibits intrusive and symplastic cell growth in developing wood cells of *Populus*. *Plant Physiology* 146: 554–565.

Sinnott EW, Bloch R. 1939. Changes in intercellular relationships during the growth and differentiation of living plant tissues. *American Journal of Botany* 26: 625–634.

Smith LG, Oppenheimer DG. 2005. Spatial control of cell expansion by the plant cytoskeleton. *Annual Review of Cell and Developmental Biology* 21: 271–295.

Snegireva AV, Ageeva MV, Amenitskii SI, Chernova TE, Ebskamp M, Gorshkova TA. 2010. Intrusive growth of sclerenchyma fibers. *Russian Journal of Plant Physiology* 57: 342–355.

Snegireva A, Chernova T, Ageeva M, Lev Yadun S, Gorshkova T. 2015. Intrusive growth of primary and secondary phloem fibres in hemp stem determines fibre bundle formation and structure. *AoB Plants* 7: plv061.

Sundell D, Street NR, Kumar M, Mellerowicz EJ, Kucukoglu M, Johnsson K, Kumar V, Mannapperuma C, Delhomme N, Nilsson O *et al.* 2017. AspWood: High-spatial-resolution transcriptome profiles reveal uncharacterized modularity of wood formation in *Populus tremula*. *Plant Cell* 29: 1585–1604.

Takeda T, Furuta Y, Awano T, Mizuno K, Mitsuishi Y, Hayashi T. 2002. Suppression and acceleration of cell elongation by integration of xyloglucans in pea stem segments. *Proceedings of the National Academy of Sciences, USA* 99: 9055–9060.

Verhertbruggen Y, Marcus S, Haeger A, Ordaz-Ortiz J, Knox J. 2009. An extended set of monoclonal antibodies to pectic homogalacturonan. *Carbohydrate Research* 344: 1858–1862.

Vissenberg K, Fry SC, Verbelen J-P. 2001. Root hair initiation is coupled to a highly localized increase of xyloglucan endotransglycosylase action in *Arabidopsis* roots. *Plant Physiology* 127: 1125–1135.

Wang C, Li S, Ng S, Zhang B, Zhou Y, Whelan J, Wu P, Shou H. 2014. Mutation in xyloglucan 6-xylosyltransferase results in abnormal root hair development in *Oryza sativa*. *Journal of Experimental Botany* 65: 4149–4157.

Wardrop AB. 1959. Cell wall formation in root hairs. *Nature* 184: 996.

Wardrop AB, Harada H. 1965. The formation and structure of the cell wall in fibres and tracheids. *Journal of Experimental Botany* 16: 356–371.

Wenham MW, Cusick F. 1975. The growth of secondary wood fibres. *New Phytologist* 74: 247–261.

Wilczek AB, Iqbal M, Włoch W, Klisz M. 2018. Geometric analysis of intrusive growth of wood fibres in *Robinia pseudoacacia*. *IAWA Journal* 39: 191–208.

Willats W, Limberg G, Buchholt H, van Alebeek G, Benen J, Christensen T, Visser J, Voragen A, Mikkelsen J, Knox J. 2000. Analysis of pectic epitopes recognised by hybridoma and phage display monoclonal antibodies using defined oligosaccharides, polysaccharides, and enzymatic degradation. *Carbohydrate Research* 327: 309–320.

Willats W, Marcus S, Knox J. 1998. Generation of a monoclonal antibody specific to $(1\rightarrow5)$-α-l-arabinan. *Carbohydrate Research* 308: 149–152.

Włoch W, Jura-Morawiec J, Kojs P, Iqbal M, Krawczyszyn J. 2009. Does intrusive growth of fusiform initials really contribute to circumferential growth of vascular cambium? *Botany-Botanique* 87: 154–163.

Yahya R, Sundaryono A, Imai T, Sugiyama J. 2015. Distance from vessels changes fiber morphology in *Acacia mangium*. *IAWA Journal* 36: 36–43.

Yanagisawa M, Desyatova AS, Belteton SA, Mallery EL, Turner JA, Szymanski DB. 2015. Patterning mechanisms of cytoskeletal and cell wall systems during leaf trichome morphogenesis. *Nature Plants* 1: 15014.

Yu Y, Wu S, Nowak J, Wang G, Han L, Feng Z, Mendrinna A, Ma Y, Wang H, Zhang X *et al.* 2019. Live-cell imaging of the cytoskeleton in elongating cotton fibres. *Nature Plants* 5: 498–504.

Zabotina OA, Avci U, Cavalier D, Pattathil S, Chou YH, Eberhard S, Danhof L, Keegstra K, Hahn MG. 2012. Mutations in multiple XXT genes of *Arabidopsis* reveal the complexity of xyloglucan biosynthesis. *Plant Physiology* 159: 1367–1384.

Zabotina OA, van de Ven WTG, Freshour G, Drakakaki G, Cavalier D, Mouille G, Hahn MG, Keegstra K, Raikhel NV. 2008. Arabidopsis XXT5 gene encodes a putative a-1,6- xylosyltransferase that is involved in xyloglucan biosynthesis. *The Plant Journal* 56: 101–115.

Zhang D, Zhang B. 2020. Pectin drives cell wall morphogenesis without turgor pressure. *Trends in Plant Science* 25: 719–722.

Supporting Information

Additional Supporting Information may be found online in the Supporting Information section at the end of the article.

Fig. S1 Cross-sectional shapes of dried macerated fibers.

Fig. S2 Fiber height profile across fiber width determined by AFM.

Fig. S3 AFM topography image showing distribution of pits in wood fibers.

Fig. S4 Distribution of cell wall matrix components and signals from secondary antibodies alone in young and mature fibers.

Fig. S5 Uniform distribution of xylan cell wall epitopes in developing and mature fibers.

Fig. S6 Uniform distribution of RGI and mannan cell wall epitopes in developing and mature fibers.

Fig. S7 Distribution of low methylesterified homogalacturonan (HG) and nonfucosylated xyloglucan (XG) epitopes at cell surfaces.

Fig. S8 Quantification of immunogold particles from TEM images of ultrathin cross-sections through developing wood fibers.

Methods S1 Simulation modeling details.

Please note: Wiley Blackwell are not responsible for the content or functionality of any Supporting Information supplied by the authors. Any queries (other than missing material) should be directed to the *New Phytologist* Central Office.